Exotic tetraquark states with two $\bar{b}$ quarks and $J^P = 0^+$ and 1^+ B_s states in a nonperturbatively tuned lattice NRQCD setup

R. J. Hudspith[*]

GSI Helmholtzzentrum für Schwerionenforschung, 64291 Darmstadt, Germany

D. Mohler[†]

GSI Helmholtzzentrum für Schwerionenforschung, 64291 Darmstadt, Germany
and Institut für Kernphysik, Technische Universität Darmstadt,
Schlossgartenstrasse 2, 64289 Darmstadt, Germany

We use $n_f = 2 + 1$ Wilson-clover gauge-field ensembles from the Coordinated Lattice Simulations (CLS) Consortium in a lattice nonrelativistic QCD (NRQCD) setup to predict the binding energy of an $I(J^P) = 0(1^+)$ $ud\bar{b}\bar{b}$ tetraquark and a $\frac{1}{2}(1^+)\ell s\bar{b}\bar{b}$ tetraquark. We determine the binding energies with respect to the relevant BB^* and $B_s B^*$ thresholds, respectively, to be 112.0(13.2) MeV for the $ud\bar{b}\bar{b}$, and 46.4(12.3) MeV for the $\ell s\bar{b}\bar{b}$. We also determine the ground-state $J^P = 0^+$ B_{s0}^* and 1^+ B_{s1} mesons to lie 75.4(14.0) and 78.7(13.9) MeV below the BK and B^*K thresholds, respectively. Our errors are entirely dominated by systematics due to discretization effects. To achieve these measurements, we performed a neural network based nonperturbative tuning of the lattice NRQCD Hamiltonian's parameters against the basic bottomonium spectrum. For all lattice spacings considered we can reproduce the continuum splittings of low-lying bottomonia. It is worth remarking that our nonperturbative tuning parameters deviate from 1 by significant amounts, particularly the term c_2.

I. INTRODUCTION

The study of doubly heavy tetraquarks with (anti)bottom quarks is currently an area of considerable interest, both on the lattice and in phenomenology. These states are of an explicitly exotic nature, and initial studies of doubly heavy $ud\bar{b}\bar{b}$ tetraquarks, e.g. [1,2] and references therein, suggest rather large binding energies.

Early lattice studies found an attractive heavy-light meson-meson potential [3–10] indicative of the possibility to admit a bound $ud\bar{b}\bar{b}$ tetraquark (T_{bb}) in nature. More recently, dynamical light-quark simulations with static b quarks [1,11–13], and with lattice nonrelativistic QCD (NRQCD) b quarks [2,14–16] have predicted a strong-interaction-stable $I(J^P) = 0(1^+)$, $ud\bar{b}\bar{b}$ tetraquark. Phenomenologically this state is almost unequivocally expected to be deeply bound [17–43] with respect to the lowest-lying noninteracting BB^* threshold.

From a diquark perspective, if a $ud\bar{b}\bar{b}$ tetraquark is deeply bound the next logical candidate with a slightly less attractive light good-diquark configuration has flavor $\ell s\bar{b}\bar{b}$ and quantum numbers $I(J^P) = \frac{1}{2}(1^+)$. Such a state has been measured on the lattice to lie below the $B_s B^*$ threshold in [2,14,44], and is somewhat more shallowly bound than the $ud\bar{b}\bar{b}$. Phenomenologically this state is expected to lie quite close to threshold [19,23,26,28,30,36–39,41–43,45–49], with the majority of relativistic quark models [50] suggesting it is in fact unbound [23,35,40].

Further states of interest are the $J^P = 0^+$ B_{s0}^* and 1^+ B_{s1} mesons. Their lighter $D_{s0}^*(2317)^\pm$ and $D_{s1}(2460)^\pm$ counterparts show properties not expected in quark-model calculations and were among the first exotic states discovered in the era of the b factories [51,52]. While a modern lattice QCD scattering calculation obtains these states significantly below the respective threshold [53] (using a relativistic formalism), other approaches obtain results consistent with [54,55] (using lattice NRQCD) [56] (using static b quarks) the lowest-lying two-meson thresholds BK and B^*K, respectively. Similar statements can be made about various phenomenological models [57–84]. Typically, relativistic quark-model calculations predict these states to lie at or above threshold, whereas other

[*]renwick.james.hudspith@googlemail.com
[†]d.mohler@gsi.de

approaches usually predict they lie below. It has been a motivation of our work to investigate the impact of the lattice NRQCD tuning on these states and provide an approach to determining these states differing from previous lattice studies.

NRQCD measurements have a long and storied history within the field of lattice QCD. They are numerically very cheap to perform and can be statistically precise. NRQCD is an effective field-theory approach to describing heavy bottom-quark (b-quark) dynamics, which however has some difficult-to-quantify systematics. Nevertheless, lattice NRQCD studies have made important contributions to standard model quantities such as α_s [85], the b-quark mass [86,87], and b-meson decays and $|V_{cb}|$ [88], to name but a few. NRQCD is but one approach to b physics. Others include relativistic heavy-quark actions [89–91], heavy-quark effective theory [92], and various extrapolation approaches [93–95]. Resolving the physical b as a valence quark with the same action as the light quarks requires a very fine lattice spacing and a large box; with current technology generating such ensembles is very expensive.

Tuning the lattice NRQCD action has periodically been of interest [96–98], particularly when it comes to choices of different tadpole improvement factors [99,100], and to whether the action's parameters should be perturbatively improved [101,102]. We will show that all coefficients of a simple truncation of the NRQCD action can be tuned entirely nonperturbatively using machine learning to reproduce the simple low-lying spectrum of bottomonia to a level compatible with the uncertainty on our lattice spacing (roughly 1%). The results for the simple spectrum including excitations from our approach will be compared to those using tree-level coefficients.

In Sec. II the lattice methodology for our calculation is described with a particular focus on the nonperturbative lattice NRQCD tuning. The results of this tuning are summarized in Sec. III, where we also present the impact of our tuning on the spectrum of low-lying bottomonium excitations. In Secs. IV A, IV B, and V we present our main physics analysis for the doubly heavy tetraquarks and B_s states, respectively. We proceed with a discussion of systematic uncertainties in Sec. VI and conclude in Sec. VII.

II. METHODOLOGY

A. NRQCD Hamiltonian and evolution

For the implementation of the $O(v^4)$ NRQCD Hamiltonian (with higher-order discretization-correction terms c_5 and c_6) we follow [96] and [103]. To obtain our heavy-quark propagator we apply the symmetric evolution to some prepared source $G(x, t)$ (technical aspects of the lattice NRQCD implementation can be found in Appendix A for the adventurous reader),

$$G(x, t+1) = \left(1 - \frac{\delta H}{2}\right)\left(1 - \frac{H_0}{2n}\right)^n \tilde{U}_t(x,t)^\dagger \left(1 - \frac{H_0}{2n}\right)^n$$
$$\times \left(1 - \frac{\delta H}{2}\right) G(x, t), \tag{1}$$

with

$$H_0 = -\frac{1}{2aM_0}\Delta^2,$$
$$H_I = \left(-c_1 \frac{1}{8(aM_0)^3} - c_6 \frac{1}{16n(aM_0)^2}\right)(\Delta^2)^2$$
$$+ c_2 \frac{i}{8(aM_0)^2}(\tilde{\Delta} \cdot \tilde{E} - \tilde{E} \cdot \tilde{\Delta}) + c_5 \frac{\Delta^4}{24(aM_0)}$$
$$H_D = -c_3 \frac{1}{8(aM_0)^2}\sigma \cdot (\tilde{\Delta} \times \tilde{E} - \tilde{E} \times \tilde{\Delta}) - c_4 \frac{1}{2(aM_0)}\sigma \cdot \tilde{B}$$
$$\delta H = H_I + H_D, \tag{2}$$

where for readability we have separated the contributions to δ_H into the spin-dependent H_D and spin-independent H_I terms. Here aM_0 is the bare b-quark mass and n is the stability parameter (which we will always set to 4 throughout this work). The tilde indicates a higher-order improved version of the derivative, tadpole improvement of the links, or improvement of the traceless clover field-strength tensor, of which E and B are the usual components [97]. Two typical choices for the tadpole-improvement factor U_0 exist in the literature: the fourth root of the plaquette U_{0P}, and the mean Landau link U_{0L}. One of the facets of this work will be to investigate the dependence of our tuning on these choices [104]. As the Hamiltonian is derived from a Taylor expansion in aM_0, results from measurements at $aM_0 \approx 1$ are not likely to be trustworthy, and this puts a constraint on how fine a lattice spacing can be used.

We will later propose a strategy to allow all of the coefficients c_i to be tuned nonperturbatively, but for now we discuss some expectations for these coefficients from the literature: the coefficient c_3 is expected to be close to 1 as there is a spin-average combination that is approximately proportional to c_3 [87] and it turns out to match experiment well when $c_3 \approx 1$. The other spin-dependent term c_4 is expected to affect most strongly the $\Upsilon - \eta_b$ hyperfine splitting [105] and plays a role in the spin-orbit splitting; typically, it has a value greater than 1. The coefficient c_2 is commonly set to its tree-level value of 1. The terms c_5 and c_6 are pure discretization-effect canceling terms for the spatial and temporal applications of H_0, respectively, and if these effects are small, should be $O(1)$. c_1 is suppressed by a further power of the mass and is expected to be close to 1 as well.

The NRQCD action is known to the next higher order ($O(v^6)$) [96,106] with coefficients $c_7...c_{11}$,

$$H_I^{v6} = -c_{10} \frac{1}{8(aM_0)^3} (\tilde{E} \cdot \tilde{E} + \tilde{B} \cdot \tilde{B})$$

$$- c_{11} \frac{1}{192(n)^2(aM_0)^3} (\Delta^2)^3$$

$$H_D^{v6} = -c_7 \frac{1}{8(aM_0)^3} \{\tilde{\Delta}^2, \sigma \cdot \tilde{B}\}$$

$$- c_8 \frac{3}{64(aM_0)^4} \tilde{\Delta}^2 \sigma \cdot (\tilde{\Delta} \times \tilde{E} - \tilde{E} \times \tilde{\Delta})$$

$$- c_9 \frac{i}{8(aM_0)^3} \sigma \cdot (\tilde{E} \times \tilde{E} + \tilde{B} \times \tilde{B}). \qquad (3)$$

Inclusion of these higher-order terms has been argued in the literature to have some small effect [97,107,108] at typical lattice spacings for bottomonia; similarly for the case of some bbb-baryon splittings they do have some significant impact [109]. We intend to see how well we can reproduce the bottomonium spectrum with just the terms listed in Eq. (2), as this will allow for a more quantitative comparison against previous works which measure related quantities. There is nothing inherently stopping us from including higher orders of the NRQCD Hamiltonian in our tuning, provided there are enough states that can be used as inputs. We address this point later in the paper in Sec. VI, where we consider adding only the tree-level spin-dependent higher-order coefficients $c_7 = c_8 = c_9 = 1$ to our tuning to probe their impact, and we will find that their inclusion does improve some of our heavy-light spin splittings. We also consider, conversely, the implications of reducing the number of tunable parameters in Appendix B and find that it worsens the quality of our tuning.

As we see from Eq. (1), lattice NRQCD incorporates corrections to the static Wilson-line propagator, so working at very coarse lattice spacings will likely include strong discretization effects from the gluon field itself, suggesting that there is an appropriate window for expecting accurate results. When investigating heavy-light B-meson physics, as we will do here, we are further constrained from additional light-quark discretization effects. As any measurement with lattice NRQCD inherently means we do not have a formal continuum limit, serious care is needed in working within an appropriate range of lattice spacings and in conservatively estimating discretization effects.

B. Nonperturbative tuning

Lattice NRQCD calculations will often either use tree-level parameters ($c_i = 1$) [2,55,103], or include a few determined at $O(\alpha_s)$ using lattice perturbation theory [101,110,111]. Occasionally, some [87,105,109] have individually tuned c_4 and/or c_3 by a nonperturbative prescription. Instead of any of these approaches we will see how precisely we can determine the simple ground-state bottomonium spectrum by allowing all of the parameters to vary

and tuning them simultaneously via a neural network. It is important to note that we will be forcing a truncated series to approximate the continuum spectrum and the parameters we determine will therefore be absorbing cutoff effects from many sources.

As lattice NRQCD has an additive mass renormalization, we cannot directly determine the masses of the pseudoscalar (η_b) or vector (Υ) mesons. Instead, the overall b-quark mass aM_0 is tuned from the nonrelativistic dispersion relation of the η_b and Υ via the expansion

$$aE(p) = aM_1 + \frac{a^2 p^2}{2aM_2} + \cdots, \qquad (4)$$

to match the kinetic mass, aM_2, to the spin-averaged continuum η_b and Υ masses. We will use the value 9.445(2) GeV for this spin average from [105]. In practice this is done by us using partially twisted boundary conditions [112,113].

The operators and their continuum analogs used in our tuning can be found in Table I; these are all taken from [114] and use the quark-line-connected contractions of the simple operators

$$O(x) = \bar{\psi} \Gamma(x) \psi, \qquad (5)$$

with Coulomb gauge-fixed [115] wall-source, sink-smeared propagators.

We have chosen the simple ground-state operators of Table I for our tuning data as there should be little ambiguity in determining their masses precisely from a correlated single-exponential fit to the resulting correlator. This allows for higher-order excitations of bottomonia to become predictions/indications of the quality of our tuning as discussed in Sec. III A. We chose to tune our parameters against the splittings with regard to the η_b of the states listed in Table I. For the continuum splittings we will use the most-recent Particle Data Group (PDG) values [116], while noting that there is some tension between the experimental determinations of the $\Upsilon - \eta_b$ hyperfine splitting.

TABLE I. Table of lattice operators used with their continuum-state analogs. Here σ_i are the usual Pauli matrices and Δ_i is the symmetric lattice finite difference.

State	PDG mass [GeV] [116]	$\Gamma(x)$
$\eta_b(1S)$	9.3987(20)	γ_5
$\Upsilon(1S)$	9.4603(3)	γ_i
$\chi_{b0}(1P)$	9.8594(5)	$\sigma \cdot \Delta$
$\chi_{b1}(1P)$	9.8928(4)	$\sigma_j \Delta_i - \sigma_i \Delta_j \ (i \neq j)$
$\chi_{b2}(1P)$	9.9122(4)	$\sigma_j \Delta_i + \sigma_i \Delta_j \ (i \neq j)$
$h_b(1P)$	9.8993(8)	Δ_i

Often studies will focus on splittings within the *S*- and *P*-wave states [114] separately, because the measured *S*-wave—*P*-wave splitting is usually quite far from its continuum value due to unknown radiative corrections and higher-order effects not accounted for. An example of this can be seen in e.g. [55], where a significant difference between the PACS-CS lattice spacing and one derived from the 1*P*-1*S* splitting was seen. The procedure of remedying this by redefining the lattice spacing after tuning aM_0 by this splitting is somewhat common in practice [117,118]. For us, it is hard to justify redetermining the lattice spacing to match a physical splitting from lattice NRQCD, and we will show with our tuning that it is possible to absorb these differences into the coefficients themselves.

We will follow our prior work of [119] where we tuned a relativistic charm-quark action nonperturbatively by using a neural network to infer the dependence of states on the action parameters. This time we will focus on the splittings of states, rather than explicit masses. A schematic of our approach is shown in Fig. 1, showing the inputs and outputs we use to train the network. It should be noted that the parameters are not universal: they will, in principle, be specific to our underlying gauge action, fermionic action, our choice of tadpole improvement factor, our choice of improvement terms in the NRQCD Hamiltonian, and even our renormalization trajectory set by the observable(s) used to define it.

We will use a network with two hidden layers of just 12 nodes. The network uses the Adam minimizer [120] with early stopping, minibatches, and an adjusted learning rate. Approximately 20% of our data are used for validation, and

we generate 100 different runs of randomly chosen lattice NRQCD coefficients per ensemble.

One may wonder if our setup in Fig. 1 is underdetermined due to having more outputs than inputs, but we observe that the coefficients are all empirically well determined. To further investigate this concern, we perform a test on ensemble A653 with fewer parameters (we fix $c_5 = c_6 = 1$) to check the general features of our tuning in Appendix B. We observe a slightly worse quality in the predicted parameters with this reduced parameter set but qualitatively similar results to our full tuning.

III. TUNING RESULTS

We will only consider gauge ensembles generated by the Coordinated Lattice Simulations (CLS) Consortium at the $SU(3)_f$-symmetric point to determine our lattice NRQCD parameters, as dynamical light pions are not expected to significantly affect the splittings considered [121]. These ensembles have a mixture of open- (U103 and H200) and periodic- (A653 and B450) temporal boundaries. All of these ensembles are $n_f = 2 + 1$ nonperturbatively improved clover-Wilson, Symanzik gauge configurations and are listed in Table II. Further details on their generation can be found in [122] and [123], with lattice spacings from [124] and an estimate for A653 from [125]. For the open-boundary configurations we sit in the middle of the lattice and compute forward and backward lattice NRQCD *b*-quark propagators away from this time slice. For the periodic-boundary configurations we only compute the forward-propagating state to allow for a larger temporal range to fit to. For the open-boundary-condition ensembles we use the plaquette for the whole gauge field in our tadpole improvement, and not one measured in the bulk.

Table III and Fig. 2 illustrate a curious result: the neural network strongly prefers a negative value of the coefficient c_2 with a significant dependence on both the lattice spacing and the choice of tadpole factor U_0. It is important to note
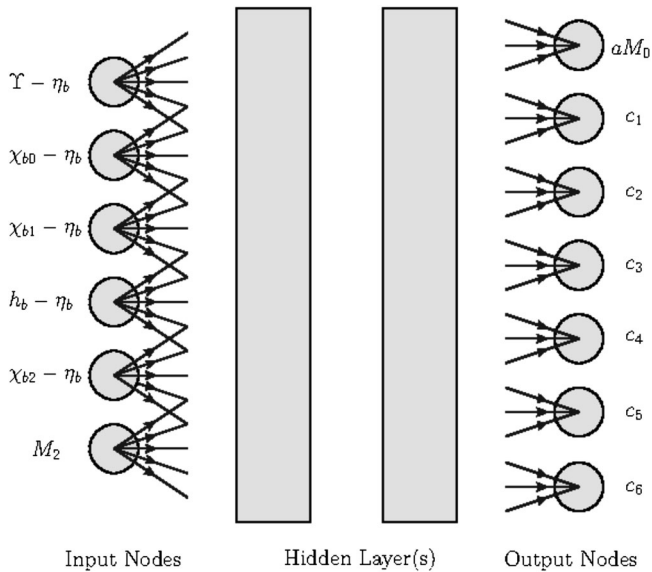

FIG. 1. Schematic picture of our setup; lines indicate weights (not all are drawn as each node is connected to each within the hidden layer) and the arrows indicate the feed-forward nature of our network.

TABLE II. Flavor $SU(3)_f$-symmetric ensembles used in this work for the nonperturbative tuning. A653* indicates tadpole improvement with the mean Landau link; all others use the fourth root of the plaquette determined from the entire lattice volume. N_{Conf} indicates the number of independent gauge configurations used and N_{Prop} indicates the number of NRQCD propagators used.

Ensemble	*T* boundary	a [fm]	U_0	$N_{\text{Conf}} \times N_{\text{Prop}}$
A653	Periodic	0.09929	0.85005	100×12
A653*	Periodic	0.09929	0.82918	100×12
U103	Open	0.08636	0.85248	500×2
B450	Periodic	0.07634	0.85812	400×8
H200	Open	0.06426	0.86153	500×2

TABLE III. Nonperturbative tuning parameters for the various $SU(3)_f$-symmetric ensembles considered in this work; bracketed values indicate the variations in the neural-network predicted parameters and not true errors. For each ensemble 100 tuning runs were performed.

Ensemble	aM_0	c_1	c_2	c_3	c_4	c_5	c_6
A653	2.0585(25)	0.611(18)	−1.255(44)	1.121(11)	0.996(10)	0.688(17)	0.701(17)
A653*	2.1088(55)	0.790(14)	−1.014(73)	1.062(15)	0.931(18)	0.700(13)	0.695(13)
U103	1.8035(32)	0.787(16)	−0.789(61)	1.057(10)	0.960(11)	0.828(13)	0.932(14)
B450	1.5542(89)	0.819(16)	−0.556(50)	1.077(13)	0.913(15)	0.861(11)	0.903(15)
H200	1.3189(19)	0.940(9)	−0.519(56)	1.027(3)	0.832(13)	0.866(10)	0.866(9)

that positive values of c_2 exist in all of our training datasets, as do the tree-level parameters, so this result is unlikely to be biased by our training data. The parameters c_1, c_5, and c_6 are the other spin-independent contributions to the NRQCD Hamiltonian and are all smaller than 1 and seem to be inversely proportional to c_2. This is further illustrated in our retuning with $c_5 = c_6 = 1$ in Appendix B where we observe that c_2 decreases when c_5 and c_6 are larger. It is evident that the tuned c_1 acts similarly as it multiplies the same operator as c_6, albeit with a different power of the bare mass and numerical prefactors.

A slightly unexpected behavior is also apparent for the determined coefficient c_4, as it is smaller than 1 for all our ensembles, suggestive of interplay between the determinations of c_2 and c_4. From our training runs we have seen that while c_2 is sensitive to the S-wave—P-wave splitting (with positive c_2 reducing this and negative c_2 enhancing it), c_4 is mostly sensitive to the hyperfine $\Upsilon - \eta_b$ (1S) splitting with a larger value of c_4 increasing this splitting. This is further supported by our results in Sec. VI where tuning to the $B^* - B$ splitting increases the 1S-hyperfine and the parameter c_4 while also making c_2 positive.

Both c_2 and c_4 show strong dependence on the choice of tadpole factor, which is unsurprising as they multiply the field-strength tensor. Oddly, the network gives the coefficient c_1 some visible tadpole dependence, implying this coefficient is being used to compensate for changes in c_2 and c_4. In our bare-mass regime (and with our chosen stability parameter) c_1 is likely one of the largest spin-independent contributions and therefore a significant handle for the neural network.

The determined coefficient c_3 is always close to 1 with some tadpole dependence and mild lattice-spacing variation. The parameters c_5 and c_6 show almost no tadpole dependence but strong lattice-spacing dependence, which is to be expected as their job is to cancel higher-order lattice artifacts.

The bare-mass tuning appears to not strongly depend on the other coefficients, only on the choice of tadpole improvement factor. This can be inferred by comparing the tuned values of aM_0 for the tree-level tuning (Table IV) with our neural network parameters (Table III), where aM_0 is more or less consistent within errors. This suggests that one can likely tune aM_0 independently of all the other parameters (with the interesting exception of A653 with the U_{0L} tadpole term). For the nonperturbatively tuned parameters we see that for U_{0P} or U_{0L} the ratio of their aM_0s is consistent with the inverse of their ratios of tadpole improvement factors.
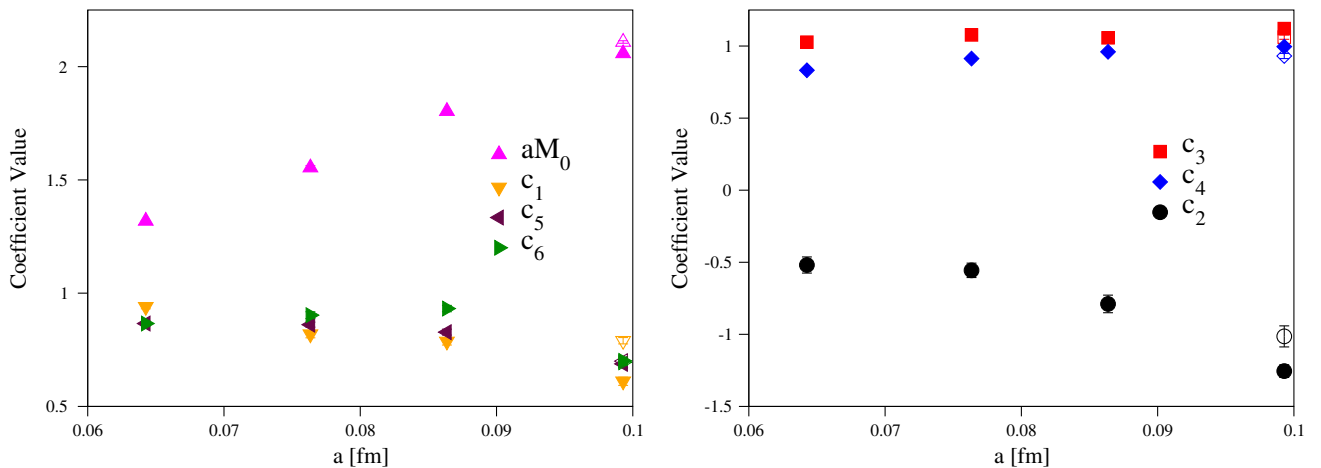

FIG. 2. Plots of the coefficient determinations (Table III) from our neural network vs the lattice spacing. Open symbols indicate the values from tuning with the U_{0L} tadpole prescription.

TABLE IV. Tree-level aM_0 tunings obtained from the spin-averaged kinetic mass by linear interpolation.

Ensemble	A653	A653*	U103	B450	H200
aM_0	2.073(16)	2.151(16)	1.812(12)	1.559(6)	1.323(9)

Figure 3 illustrates our ability to reproduce the experimental low-lying S- and P-wave splittings for bottomonia in comparison to tree-level NRQCD for different lattice spacings. Apart from our tuning being consistent with experiment, we note some interesting features: tree-level NRQCD's approach to the continuum for the $1P$-$1S$ splittings appear to be linear with the lattice spacing, indicating that on these lattices it will never be accurately reproduced within the applicability window of NRQCD. For our neural network tuning χ_{b0} appears slightly too heavy, and χ_{b2} too light, with χ_{b1} and h_b matching experiment much better. This could be a sign of missing higher-order terms in our NRQCD implementation as
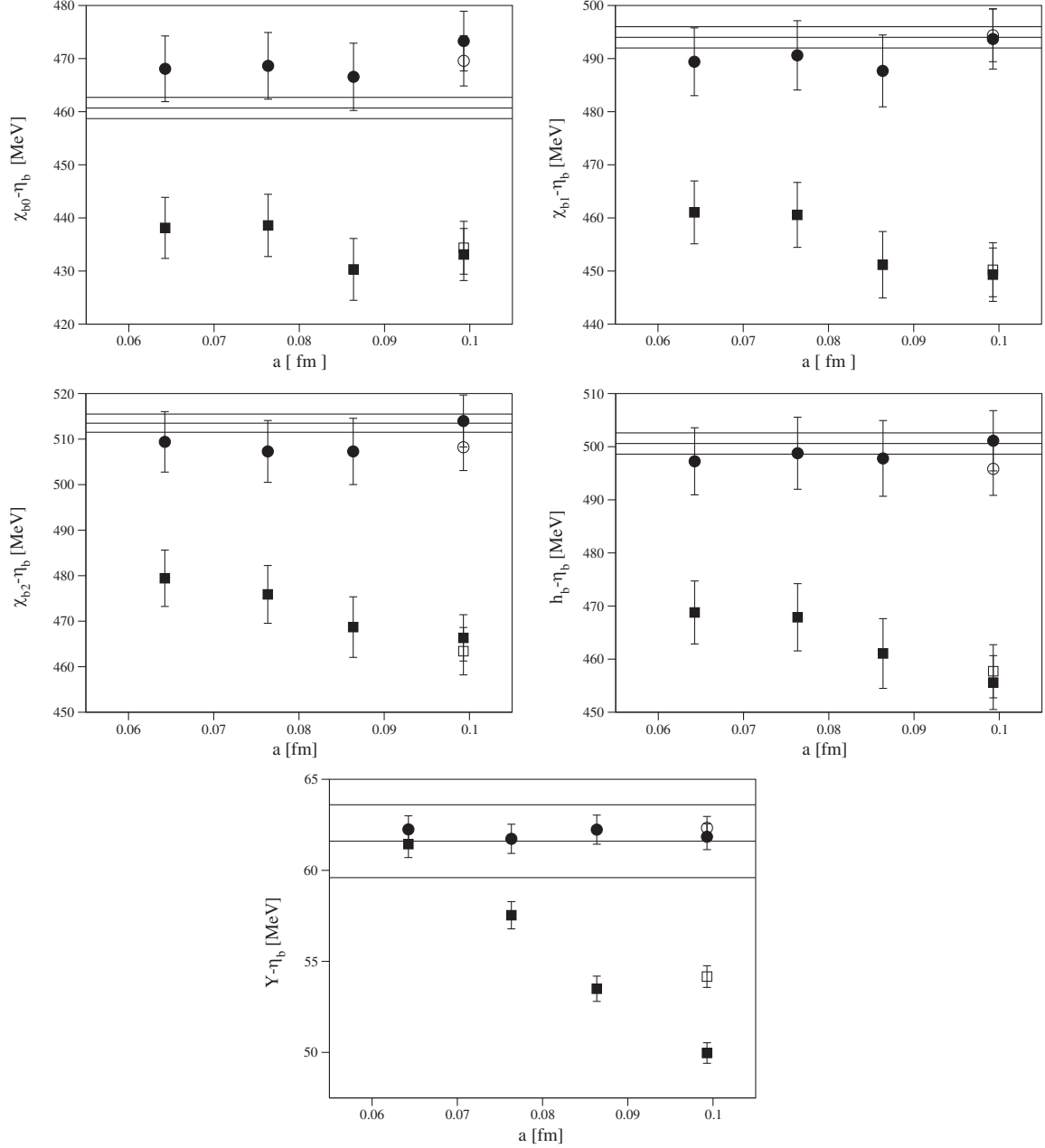

FIG. 3. Measured splittings from our tuning (circles) vs those obtained from using tree-level coefficients (squares). Open symbols illustrate the use of the mean Landau-link tadpole improvement term, closed symbols from the fourth root of the plaquette. Horizontal lines indicate the PDG values for these splittings.

TABLE V. Average absolute percentage deviation "D," Eq. (6), from our target continuum splittings.

Ensemble	A653	A653*	U103	B450	H200
NN-tuned	0.7%	1.0%	1.1%	0.8%	1.0%
Tree-level	10.4%	9.0%	9.0%	6.4%	5.0%

TABLE VI. Gaussian smearing widths α used at source and sink to create the GEVP of Eq. (7) as well as the number of configurations and NRQCD bottom propagators used.

Ensemble	$N_{\mathrm{Conf}} \times N_{\mathrm{Prop}}$	1	2	3	4
A653	500×48	2.5	5	10	20
U103	500×16	2.5	5	10	20
B450	400×32	4	8	16	32
H200	500×8	4	8	16	32

this feature seems independent of the lattice spacing. Finally, we note that for the tree-level parameters' results with the tadpole factor U_{0L} there is better agreement with the experimental hyperfine splitting than for those using U_{0P}. The two choices of tadpole-improvement factor for tree-level NRQCD are, however, equally poor for the splittings between the P-wave states and the η_b. Whichever tadpole-improvement factor is used is completely irrelevant with the neural network tuning as the choice gets absorbed into the nonperturbative coefficients.

We investigate our ability to reproduce the continuum spectrum via the simple absolute percentage deviation metric

$$D = \frac{100}{N} \sum_i^N \left| \frac{\bar{S}_i^{\mathrm{Latt.}} - \bar{S}_i^{\mathrm{Cont.}}}{\bar{S}_i^{\mathrm{Cont.}}} \right|, \qquad (6)$$

with $\bar{S}^{\mathrm{Latt.}}$ being the average value of one of our splittings and $\bar{S}^{\mathrm{Cont.}}$ being the expected central value of its continuum counterpart. We present results comparing our states from our predicted parameters with those from the tree-level tuning in Table V; the approach to the continuum for each of our splittings can be also be seen in Fig. 3.

Table V illustrates quite clearly that the tree-level parameters do appear to approach the continuum experimental spectrum, albeit very slowly. Our nonperturbative tuning never deviates in central value by more than 1.1% on average and within the experimental and lattice errors the agreement is near absolute. Of course, this is the intention of our tuning but it is worth noting that at the simple truncation of the NRQCD Hamiltonian such a reproduction of experiment is possible and a tuning with higher-order coefficients against this set of states will be unlikely to provide much improvement, and may not be well constrained.

A. Excited states of bottomonium

As we have already seen in Fig. 3, tree-level Lattice NRQCD's ability to replicate even the basic $1P$-$1S$ splittings is poor and it seems unlikely that their excited counterparts' determination will be much better. In this section we consider the excited S-wave $\eta_b(3S/2S)$, $\Upsilon(3S/2S)$ and P-wave $\chi_{b0}(3P/2P)$, $\chi_{b1}(3P/2P)$, $\chi_{b2}(3P/2P)$, and $h_b(3P/2P)$ states' splittings with respect to the $\eta_b(1S)$, and compare these to their PDG continuum counterparts where known.

For the determination of our excited states we choose to create a symmetric generalized eigenvalue problem (GEVP) [126–128] from a matrix of correlation functions constructed with different Gaussian source (first S) and sink (second S) smearings:

$$\begin{pmatrix} S_1S_1 & S_1S_2 & S_1S_3 & S_1S_4 \\ S_2S_1 & S_2S_2 & S_2S_3 & S_2S_4 \\ S_3S_1 & S_3S_2 & S_3S_3 & S_3S_4 \\ S_4S_1 & S_4S_2 & S_4S_3 & S_4S_4 \end{pmatrix}. \qquad (7)$$

As was the case in the tuning we use Coulomb gauge-fixed wall sources, where for the source we simply apply an arbitrary function, and for the sink we apply the convolution methodology outlined in the appendixes of [119]. Each "S" denotes a different smearing radius (squared), which we will call α, as illustrated in Table VI. We are primarily interested in the lowest three states, with the fourth typically lying above the $B\bar{B}$ threshold, and expected to have contamination from higher states. We solve this GEVP and diagonalize the correlator matrix for a specific "diagonalization time" [129] to obtain our principal correlators, which we then perform a correlated single-exponential fit to. Here, we needed increased statistics in comparison to our tuning runs (Table II) to be able to stably resolve the higher levels. For the P-wave states the calculation is quite complicated as the source has a derivative and must be matched similarly at the sink, and contracted with a propagator with smearing at the same source and sink going backwards; hence, many lattice NRQCD propagators are needed for these states.

Figure 4 illustrates the excited S- and P-wave state splittings with respect to the $\eta_b(1S)$. As we have already seen earlier in this section, the tree-level coefficients underestimate the $1P$-$1S$ splitting. However, their $2P$-$1S$ splitting is closer to experiment and the $3P$-$1S$ is again lower. This well-behaved $2P$-$1S$ splitting of tree-level lattice NRQCD is likely a coincidence as the $2P$-$1P$ splitting is significantly overestimated as the lattice spacing decreases. In comparison, the neural network tuning for the $2P$-$1S$ splitting is consistent with experiment and the spread of results over our lattice spacings is much more narrow. For the $2S$-$1S$ and $3S$-$1S$ splittings the spread of
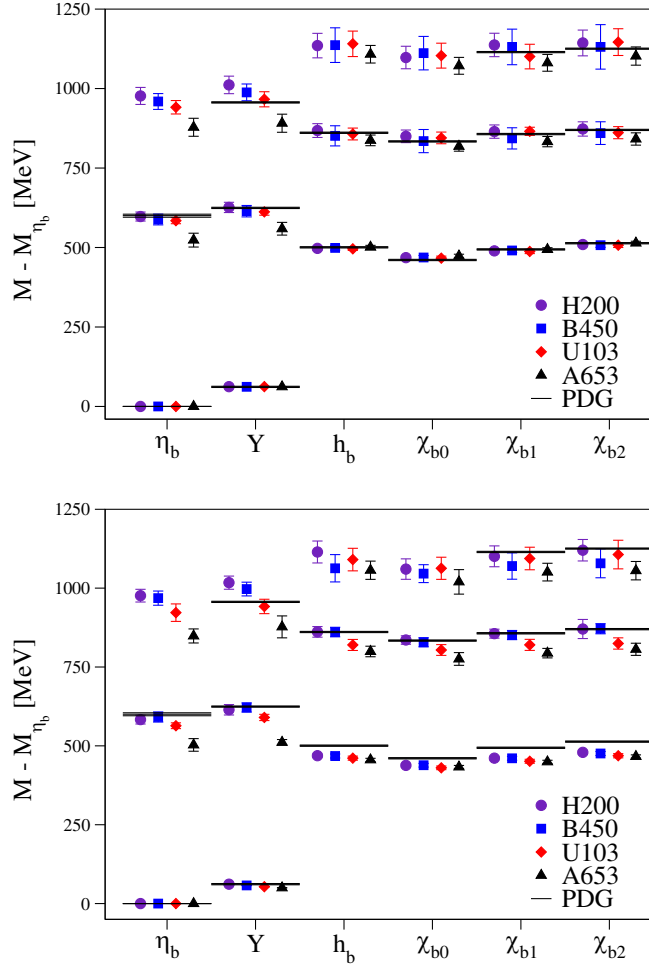
FIG. 4. *S*-wave and *P*-wave splittings of bottomonia with respect to the η_b from the neural network tuning (top) and the tree-level coefficients (bottom). Shown are the 1*S*, 2*S*, 3*S*, and 1*P*, 2*P*, and 3*P* splittings as well as their values from the PDG.

values is again smaller for the neural network, which illustrates that some discretization effect is being treated better in our tuning. The variation in errors is indicative of some of the ambiguities in finding a good fit range for these states, and the results presented in this section have errors which are statistical only and intended to be indicative rather than quantitative.

IV. EXOTIC DOUBLY HEAVY TETRAQUARK STATES

Table VII gives the ensembles used for the analysis of tetraquarks and B_s mesons, and in terms of statistics at least 6000 light, strange, and bottom propagators were used for each ensemble. In the following we will primarily consider only the coarse CLS "1" lattice spacing and use an ensemble at the finer "2" lattice spacing for comparison of discretization effects. We will consider two mass

TABLE VII. Ensemble details and gathered statistics used in our study of doubly heavy tetraquarks and exotic B_s mesons. N_{Conf} indicates the number of independent gauge configurations used and N_{Prop} indicates the number of propagators (light, strange, and $2 \times$ bottom) generated per configuration.

Ensemble	Mass trajectory	$L^3 \times L_T$	$N_{\mathrm{Conf}} \times N_{\mathrm{Prop}}$
U103	$\mathrm{Tr}[M] = C$	$24^3 \times 128$	1000×23
H101	$\mathrm{Tr}[M] = C$	$32^3 \times 96$	500×12
U102	$\mathrm{Tr}[M] = C$	$24^3 \times 128$	732×18
H102	$\mathrm{Tr}[M] = C$	$32^3 \times 96$	500×16
U101	$\mathrm{Tr}[M] = C$	$24^3 \times 128$	600×18
H105	$\mathrm{Tr}[M] = C$	$32^3 \times 96$	500×16
N101	$\mathrm{Tr}[M] = C$	$48^3 \times 128$	537×18
C101	$\mathrm{Tr}[M] = C$	$48^3 \times 96$	400×16
H107	$\widetilde{m}_s = \widetilde{m}_s^{\mathrm{Phys}}$	$32^3 \times 96$	500×16
H106	$\widetilde{m}_s = \widetilde{m}_s^{\mathrm{Phys}}$	$32^3 \times 96$	500×16
H200	$\mathrm{Tr}[M] = C$	$32^3 \times 96$	500×28

trajectories: one where the sum of the quark masses $\frac{2}{\kappa_l} + \frac{1}{\kappa_s}$ is constant as proposed in [130] and one where the renormalized strange-quark mass $\widetilde{m}_s \approx \widetilde{m}_s^{\mathrm{Phys}}$. is kept approximately constant [131]. Both of these quark-mass trajectories use the same underlying gauge and quark action and should agree at the physical pion-mass point. With regard to the range of pion masses covered, we will use ensembles from the quark $\mathrm{SU}(3)_f$-symmetric mass point $m_\pi \approx 420$ MeV down to $m_\pi \approx 220$ MeV. More details on the generation of these ensembles can be found in [123] and [132].

From e.g. [2,14,15] it has been observed that the dependence of the binding of the tetraquark states discussed in the following sections is approximately linear in m_π^2, so the pion-mass range encompassed by our study is suitable to obtain an extrapolated result at the physical pion mass. In this work we make use of the dimensionless quantity $\phi_2 = 8t_0 m_\pi^2$ (with t_0 measured on each ensemble) as it has less uncertainty than the dimensionful physical pion mass, due to the error on the lattice spacing from [124]. The ensembles used in our study span a large range of $m_\pi, m_\pi L$, and $m_K L$ which helps us control finite-volume and chiral-extrapolation systematics.

In the next sections we again use Coulomb gauge-fixed wall sources with Gaussian smeared sinks, and primarily focus on results from the 1 lattice spacing ensembles. We will use a fixed physical sink-smearing $\alpha = 22$ for the tetraquark correlators, and a slightly larger choice $\alpha = 25$ for the B and B_s mesons. We use comparable physical choices of α for the cross-check at the finest lattice spacing on ensemble H200.
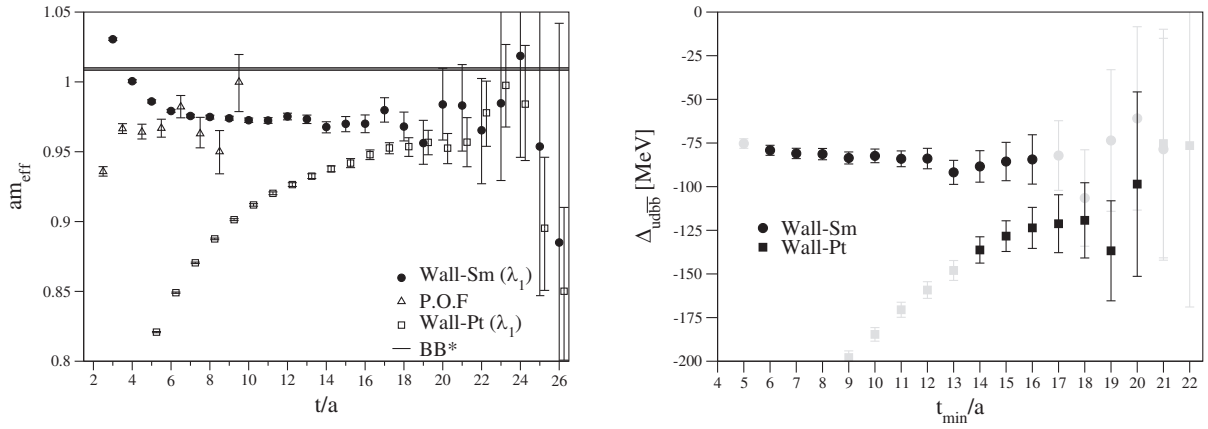
FIG. 5. Left: comparison on ensemble U103 of the effective masses of the lowest-lying principal correlator for gauge-fixed wall source with point (Wall-Pt) or smeared (Wall-Sm) sink or from the 2×2 pencil-of-functions (P.O.F) of a single Wall-Pt correlator. The data have been shifted for clarity. Right: dependence of the fit results on the lower fit bound (at fixed large upper fit bound) for a single-exponential fit for both smeared-sink and point-sink; grayed-out points indicate poor fit quality.

A. Determining the binding energy for a $ud\bar{b}\bar{b}$ tetraquark

To arrive at precise and accurate results, systematic uncertainties on the predictions of the proposed deeply bound $I(J^P) = 0(1^+)$, $ud\bar{b}\bar{b}$ tetraquark is of considerable interest. Indeed, currently the main goal of the community is to systematically improve calculations to the point where consensus can be reached on the mass of this state. In this context, it is important to investigate the size of discretization effects, and the impact of the heavy-quark formalism employed.

We start by calculating a 4×4 matrix of correlators built from quasilocal operators to determine the lowest-lying tetraquark ground state, as in [133]:

$$D = (u_a^T C\gamma_5 d_b)(\bar{b}_a C\gamma_i \bar{b}_b^T),$$
$$E = (u_a^T C\gamma_t\gamma_5 d_b)(\bar{b}_a C\gamma_i\gamma_t \bar{b}_b^T),$$
$$M = (\bar{b}\gamma_5 u)(\bar{b}\gamma_i d) - [u \leftrightarrow d],$$
$$N = (\bar{b}Iu)(\bar{b}\gamma_5\gamma_i d) - [u \leftrightarrow d]. \quad (8)$$

We will not use an operator that looks like B^*B^*, and subsequently this expected state will not be seen in our GEVP. From a preliminary study it seems like this state overlaps more strongly with extended, derivative-type operators.

As we use a nonsymmetric operator setup for the GEVP, we cannot guarantee that the resulting eigenvalues are real (in turns out that they are, well into the region where the signal degrades). We choose to approximately diagonalize the correlator matrix using the left and right eigenvectors of the GEVP at a specific "diagonalization time" [14,133,134]. We then determine the principal correlators from the diagonal of this matrix, performing

a correlated fit to a single-exponential ansatz of the lowest-lying state at sufficiently large separations to determine our tetraquark mass.

Figure 5 illustrates the danger in using a single-exponential fit to gauge-fixed wall-source and point-sink data for this $ud\bar{b}\bar{b}$ tetraquark. We chose ensemble U103 for this comparison, as it has the highest statistics. Clearly, the effective mass for the Wall-Pt data is still trending upward as the signal is lost, whereas for the Wall-Sm determination good stability is seen over a large range in time. The right "fit-stability" plot illustrates that with noisy data it is quite easy to find a good-quality fit (in terms of χ^2/dof and p value) over a small range and end up with a deeper value of the binding, and an unforeseen associated systematic. A two-exponential fit to the point-sink data is consistent with the smeared-sink determination, and the smeared-sink determination is also consistent with a 2×2 generalized pencil-of-functions [135,136] analysis of the point-sink diquark/antidiquark correlator from operator D.

Figure 6 shows an exemplary effective-mass plot of the four eigenvalues obtained from the GEVP for the ensemble N101, as well as the fit to determine the $ud\bar{b}\bar{b}$ tetraquark mass and a line of the measured lowest-lying noninteracting BB^* threshold. In all cases our second eigenvalue λ_1 is consistent with this threshold. The optimal smearing α for the $ud\bar{b}\bar{b}$ tetraquark is suboptimal for the BB^* threshold as there is still some visible excited-state contamination making this second level approach from below. It is this difference in excited-state contamination that makes a determination of the binding through a ratio of the lowest eigenvalue and the expected threshold dangerous for this data; therefore, we do not perform such an analysis.

Figure 7 shows the combined chiral and infinite-volume extrapolation of the mass of the ground state from the GEVP (the data of which are tabulated in Table VIII), after
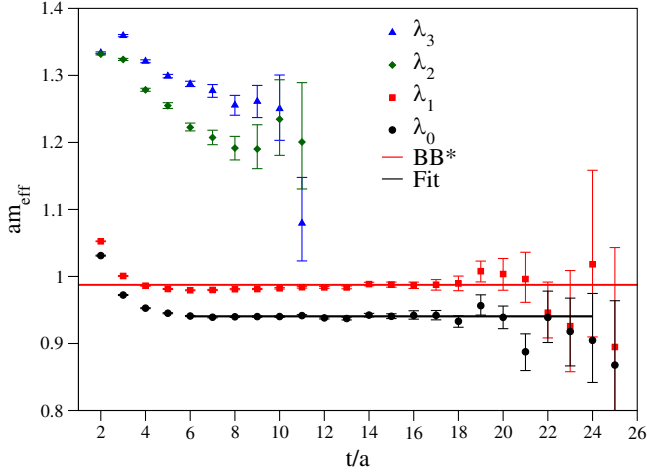
FIG. 6. Eigenvalue effective masses for ensemble N101. In addition to the effective masses, the fit determination for the mass of the $ud\bar{b}\bar{b}$ tetraquark is shown as the black line and our determination of the first noninteracting BB^* level is shown as a red line.
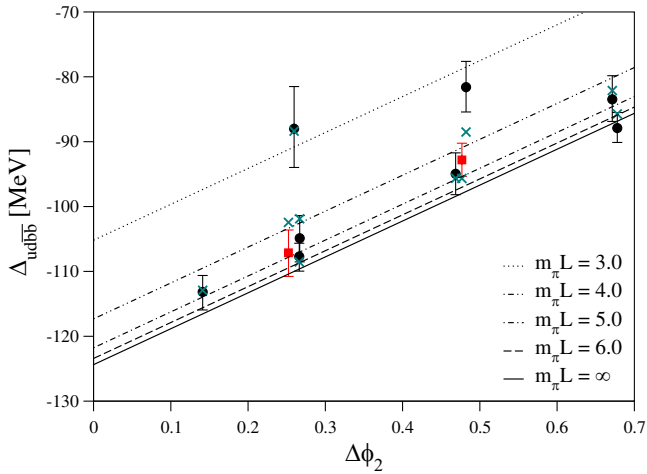

FIG. 7. Chiral and infinite-volume extrapolations of the $ud\bar{b}\bar{b}$ tetraquark; black points indicate the $\text{Tr}[M] = C$ data and red squares indicate the $\widetilde{m_s} = \widetilde{m_s}^{\text{Phys}}$. trajectory. Lines of exemplary constant $m_\pi L$ are also plotted. Teal stars indicate the central value of the fit corresponding to the point at the same ϕ_2.

subtracting the BB^* mass (which cancels the additive mass renormalization from NRQCD). We use the following ansatz for a deeply bound state:

$$
\begin{aligned}
&\Delta_{ud\bar{b}\bar{b}}(\Delta\phi_2, m_\pi L, a) \\
&= \Delta_{ud\bar{b}\bar{b}}(0, \infty, a)(1 + A\Delta\phi_2 + Be^{-m_\pi L}),
\end{aligned} \quad (9)
$$

with $\Delta_{ud\bar{b}\bar{b}}(0, \infty, a), A$, and B being shared fit parameters between the two sets of mass trajectories (as we expect minimal sea-strange contributions to this quantity), and

TABLE VIII. Measurements necessary for the $ud\bar{b}\bar{b}$ tetraquark candidate. Here, m_π has been measured directly within this dataset.

Ensemble	ϕ_2	$m_\pi L$	$B^* - B$ [MeV]	$\Delta_{ud\bar{b}\bar{b}}$ [MeV]
U103	0.7496	4.33	36.9(0.6)	−83.5(3.4)
H101	0.7561	5.83	35.3(1.0)	−87.9(2.3)
U102	0.5604	3.74	36.1(1.1)	−81.6(3.7)
H102	0.5469	4.93	34.8(1.0)	−95.0(3.2)
U101	0.3378	2.88	33.1(0.9)	−88.0(6.5)
H105	0.3451	3.91	36.3(0.8)	−104.9(3.5)
N101	0.3445	5.86	35.7(0.6)	−107.7(2.1)
C101	0.2195	4.66	33.9(0.7)	−113.2(2.7)
H107	0.5550	5.12	40.8(1.1)	−92.8(2.7)
H106	0.5550	3.88	39.1(1.0)	−107.1(3.5)
H200	0.7469	4.32	34.3(0.6)	−71.9(2.6)

$\Delta\phi_2 = \phi_2^{\text{Lat}} - \phi_2^{\text{Phys}}$ being the difference between the lattice-measured dimensionless ϕ_2 and its physical value. For the isosymmetric "physical" pion mass we use the value of 134.8 MeV recommended in [137] and for the physical t_0 we use the value determined by the Flavor Lattice Averaging Group (FLAG) [138,139]. We note that finite-volume effects here are significant and the deviation from our infinite-volume result in the chiral limit and that of $m_\pi L = 4$ is still a 5.6% correction.

From our extrapolation we obtain the binding energy at the 1 lattice-spacing,

$$
\Delta_{ud\bar{b}\bar{b}}(0, \infty, a = 0.08636 \text{ fm}) = -124.4(2.7) \text{ MeV}. \quad (10)
$$

The fit that produced this result has $\chi^2/\text{dof} = 1.2$. We note that our extrapolation to physical pion mass could have higher-order contributions, so we fit Eq. (9) with an extra term of $(\Delta\phi_2)^{3/2}$ or $(\Delta\phi_2)^2$, both of which can describe our data reasonably well and give values for $\Delta_{ud\bar{b}\bar{b}}(0, \infty, a = 0.08636 \text{ fm})$ of $-133.4(6.7)$ and $-131.9(5.5)$, respectively. For our final result we use Eq. (10) as the two higher-order fits do show some signs of overfitting, and add half the difference of the larger result as a systematic, which we denote χ. We do not have the precision or number of ensembles to fit a higher-order finite-volume correction term in combination with the one we already have. Upon removing ensembles from our fit with $m_\pi L < 4$ our result did not change within statistical errors.

Due to the reasonably large discrepancy between the results on ensembles H200 and U103 of 11.6 MeV, we decide to add half of this difference to the central value of Eq. (10) and use all of this difference as an uncertainty estimate, such that our error encompasses the coarser and finer lattice-spacing result. Later on in Sec. VI we

see a reasonably strong, positive, linear dependence of $\Delta_{ud\bar{b}\bar{b}}(0, \infty, a)$ on the $B^* - B$ splitting. As our tuning underpredicts this splitting (particularly for the $\text{Tr}[M] = C$ trajectory), we add 6.6 MeV (obtained from a linear interpolation of the data in Fig. 11 to the physical $B^* - B$) to our determination (incorporating half of this correction as a systematic for our final error) to correct for this, giving our final result:

$$\Delta_{ud\bar{b}\bar{b}}(0, \infty, 0)$$
$$= -112.0(2.7)_{\text{Stat}}(4.5)_\chi(11.6)_a(3.3)_{B^*-B} \text{ MeV}. \quad (11)$$

We observe that our data suggest the $a \to 0$ limit corresponds to a shallower binding, although the resulting state is still deeply bound and strong-interaction stable. It is clear that our estimate is dominated by systematics relating to discretization effects, where the $a \to 0$ limit is not well controlled in lattice NRQCD.

B. On the existence of an $\ell s\bar{b}\bar{b}$ tetraquark

We now briefly turn our attention to a possible $\ell s\bar{b}\bar{b}$ tetraquark (T_{bbs}), predicted from lattice QCD in [2,14], and [44] to lie around 90 MeV below the lowest-lying noninteracting two-meson threshold. This value from the literature seems already quite large as our $ud\bar{b}\bar{b}$ tetraquark is bound by roughly this magnitude and is expected to be more deeply bound due to the good light-diquark ud configuration. In addition to the $\ell s\bar{b}\bar{b}$ tetraquark state, there are now two very close-by meson-meson states at the $B_s B^*$ and $B_s^* B$ thresholds, and hence finite-volume effects may be nontrivial. As discussed earlier, most phenomenological studies agree on the existence of a $ud\bar{b}\bar{b}$ tetraquark below threshold, while fewer have considered the $\ell s\bar{b}\bar{b}$.

For this calculation we will investigate results from a 5×5 GEVP of the following quasilocal meson-meson operators with quantum numbers $I(J^P) = \frac{1}{2}(1^+)$:

$$M = (\bar{b}\gamma_5 u)(\bar{b}\gamma_i s), \qquad N = (\bar{b}Iu)(\bar{b}\gamma_5\gamma_i s)$$
$$O = (\bar{b}\gamma_5 s)(\bar{b}\gamma_i u), \qquad P = (\bar{b}Is)(\bar{b}\gamma_5\gamma_i u)$$
$$Q = \epsilon_{ijk}(\bar{b}\gamma_j u)(\bar{b}\gamma_k s). \quad (12)$$

Although we include an operator resembling $B^* B_s^*$ we will again have trouble identifying this expected level in our GEVP. For all of our ensembles we find (as in nature) that $B_s B^*$ is the lowest-lying noninteracting two-meson threshold, and we determine the mass difference $\Delta_{\ell s\bar{b}\bar{b}}$ with regard to this threshold.

Figure 8 shows the effective masses of the eigenvalues for the $\widetilde{m_s} = \widetilde{m_s}^{\text{Phys}}$ ensemble H106 as well as the two lowest-lying two-meson noninteracting thresholds $B_s B^*$ and $B B_s^*$, which are practically degenerate for this ensemble. As was the case for the $ud\bar{b}\bar{b}$, λ_1 is consistent with our
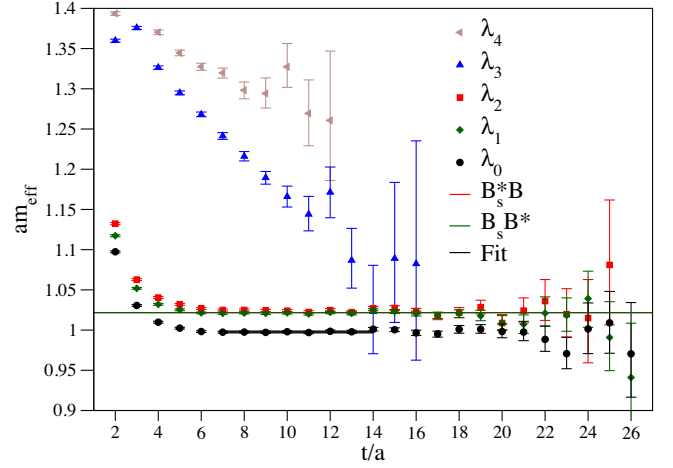

FIG. 8. Eigenvalue effective masses for ensemble H106. The fit determination for the mass of the $\ell s\bar{b}\bar{b}$ tetraquark is shown as the black line and the determinations of the first two noninteracting levels $B_s B^*$ and $B_s^* B$ are shown as (almost identical) red and green lines, respectively.

lowest-lying noninteracting threshold state. We have two close-together levels above the ground state which appear to correspond to $B_s B^*$ and $B B_s^*$. Our fourth level, λ_3, is poorly determined, suggesting that our basis needs improvement to capture the expected $B^* B_s^*$ level. Either way, these levels are reasonably far from the ground-state tetraquark candidate.

Figure 9 and Table IX show the lattice data with broken $SU(3)_f$, as these are the only ensembles we include in our fit. From these data we can see that as the strange quark becomes heavier and the light quark lighter the attractiveness of the good light-diquark diminishes. As the
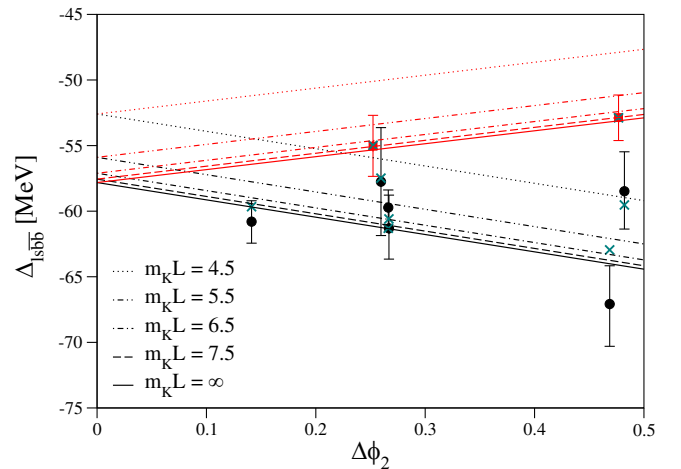

FIG. 9. Combined chiral and infinite-volume extrapolations of the $\ell s\bar{b}\bar{b}$ tetraquark. Red indicates the separate $\widetilde{m_s} = \widetilde{m_s}^{\text{Phys}}$. mass trajectory. Lines of exemplary constant $m_K L$ are also plotted. Teal stars indicate the central value of the fit corresponding to the point at the same ϕ_2.

TABLE IX. Results for the binding energy of the $\ell s\bar{b}\bar{b}$ tetraquark candidate.

Ensemble	$m_K L$	$B_s^* - B_s$	$\Delta_{\ell s\bar{b}\bar{b}}$ [MeV]
U102	4.61	37.6(1.1)	$-58.5(2.9)$
H102	6.10	35.8(1.8)	$-67.1(3.1)$
U101	4.82	37.1(1.1)	$-57.8(4.2)$
H105	6.44	35.8(1.8)	$-61.3(2.6)$
N101	9.69	38.4(0.6)	$-59.7(1.3)$
C101	9.87	36.9(0.8)	$-60.8(1.5)$
H107	7.61	41.6(0.8)	$-52.9(1.7)$
H106	7.21	38.8(0.8)	$-55.0(2.4)$

TABLE X. B_{s0}^* and B_{s1} meson mass splittings with regards to their respective measured, expected, noninteracting thresholds BK and B^*K.

Ensemble	$\Delta_{B_{s0}^*}$ [MeV]	$\Delta_{B_{s1}}$ [MeV]	$B_{s0}^* - B_{s1}$ [MeV]
U103	$-78.5(5.2)$	$-85.2(5.4)$	$-30.1(1.5)$
H101	$-49.8(6.0)$	$-55.7(6.1)$	$-29.4(2.5)$
U102	$-91.6(7.3)$	$-90.9(7.7)$	$-36.9(3.5)$
H102	$-61.3(6.0)$	$-62.1(6.9)$	$-33.9(2.7)$
U101	$-78.5(5.4)$	$-84.2(5.1)$	$-27.4(2.0)$
H105	$-59.2(5.2)$	$-70.1(7.6)$	$-39.8(6.7)$
N101	$-57.9(4.1)$	$-63.2(4.5)$	$-30.4(2.7)$
C101	$-63.7(2.9)$	$-65.8(3.8)$	$-34.4(2.0)$
H107	$-101.2(6.5)$	$-110.4(7.1)$	$-31.7(2.5)$
H106	$-90.4(5.1)$	$-96.6(5.1)$	$-32.9(2.2)$
H200	$-92.2(7.0)$	$-98.6(6.8)$	$-27.9(2.2)$

physical ($m_K L$) volume increases the state becomes more deeply bound, as was the case for the $ud\bar{b}\bar{b}$.

We fit the data displayed in Fig. 9 and tabulated in Table IX to the combined chiral/infinite-volume ansatz:

$$\Delta_{\ell s\bar{b}\bar{b}}(\Delta\phi_2, m_K L, a) = \Delta_{\ell s\bar{b}\bar{b}}(0, \infty, a)(1 + A\Delta\phi_2 + Be^{-m_K L}), \quad (13)$$

where the mass coefficient A is now different for the two mass trajectories as sea and valence strange content is expected to be important. The parameters $\Delta_{\ell s\bar{b}\bar{b}}(0, \infty, a)$ and B are again shared between the two trajectories. This fit has $\chi^2/\text{dof} \approx 1$. An extrapolation in $8\Delta t_0 m_K^2$ instead has effectively the same χ^2/dof and is entirely consistent with our final extrapolation result of $-57.8(2.4)$. A fit with $e^{-m_\pi L}$ has a slightly worse $\chi^2/\text{dof} \approx 1.2$ and a larger central value $[-59.7(2.2)]$; a fit without a finite-volume term has $\chi^2/\text{dof} \approx 1.1$ with again a slightly larger central value $-59.1(2.1)$. As neither the fits with $e^{-m_K L}$ nor $e^{-m_\pi L}$ have good significance for the parameter B, we choose to quote the average between their results and add half their difference as a finite-volume systematic. We note that given the quality of the data combined with the requirement of having more free fit parameters, it was not possible to fit higher-order terms in $\Delta\phi_2$. Our final result did not change within errors upon enforcing a cut of $m_K L > 5$.

This fit at fixed 1 lattice spacing gives the infinite-volume chiral-limit result:

$$\Delta_{\ell s\bar{b}\bar{b}}(0, \infty, a = 0.08636 \text{ fm}) = -58.8(2.4)_{\text{Stat}}(1.0)_{\text{FV}} \text{ MeV}. \quad (14)$$

Again, taking the deviation between H200 and U103 as our lattice-spacing systematic [140] and considering that our $B_s^* - B_s$ splitting is similarly as poor as our $B^* - B$ we perform the same two shifts as in the $ud\bar{b}\bar{b}$ case, yielding our final result:

$$\Delta_{ud\bar{b}\bar{b}}(0, \infty, 0) = -46.4(2.4)_{\text{Stat}}(1.0)_{\text{FV}}(11.6)_a(3.3)_{B_s^* - B_s} \text{ MeV}, \quad (15)$$

which is much less deeply bound than the previous lattice determinations of [2,14,44], but was already hinted at in [133] and is consistent with the phenomenological predictions of [19,30], and [36]. A shallow binding such as this poses a significant challenge for experimental detection.

V. THE FATE OF THE SCALAR AND AXIAL B_s MESONS

During our investigation of the $ud\bar{b}\bar{b}$ tetraquark it came to our attention that on the $SU(3)_f$-symmetric ensemble "U103" the positive-parity B mesons with the simple local operators,

$$B_{s0}^* = (\bar{b}Is), \qquad B_{s1} = (\bar{b}\gamma_i\gamma_t s), \quad (16)$$

lie below the expected BK and B^*K thresholds [141], respectively. This was not necessarily expected, as a previous finite-volume calculation of these states with different techniques [53] required the inclusion of explicit meson-meson interpolating fields to observe a state below threshold. In the following investigation of these excited B_s mesons we simply use the same wall-source/smeared-sink mesons that were computed in the previous sections' $ud\bar{b}\bar{b}$ and $\ell s\bar{b}\bar{b}$ determinations.

Table X gives the numerical results for the difference between the B_{s0}^* and BK threshold, denoted $\Delta_{B_{s0}^*}$, and the difference between the B_{s1} and B^*K, denoted $\Delta_{B_{s1}}$. We also give our measured difference between the B_{s0}^* and B_{s1}.

In Fig. 10 we show the combined chiral/infinite volume extrapolation of the binding energy for the scalar and axial
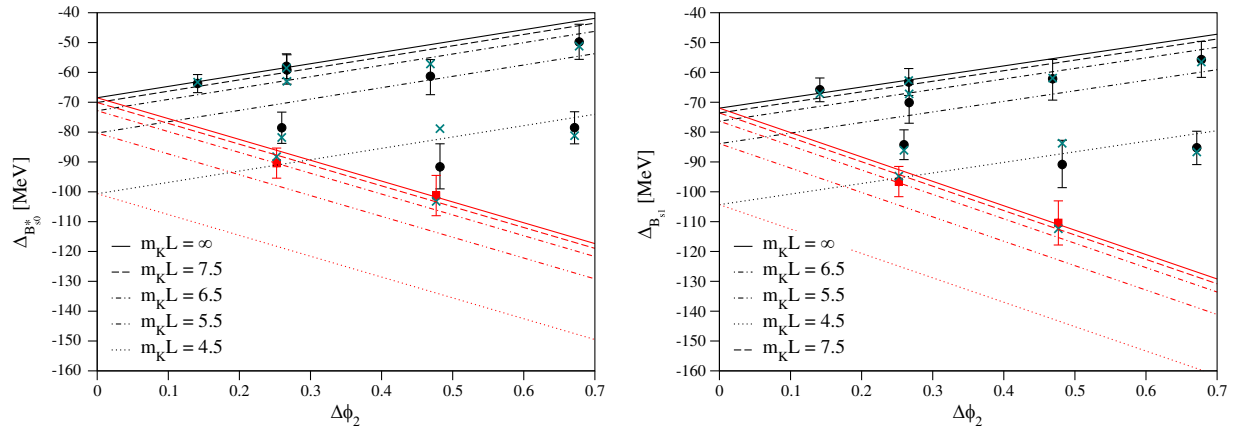
FIG. 10. Left: scalar B_{s0}^* combined chiral and infinite-volume extrapolation. Right: axial-vector B_{s1} combined chiral and infinite-volume extrapolation. Illustrative lines of constant $m_K L$ are displayed and red indicates the results from the $\widetilde{m}_s = \widetilde{m}_s^{\text{Phys}}$ trajectory. Teal stars indicate the central value of the fit corresponding to the point at the same $\Delta\phi_2$.

B_s mesons, from the neural network tuned b quarks. Here we used the same simple-fit ansatz from the previous sections for the bound-state system of both splittings:

$$\Delta_{B_{s0}^*/B_{s1}}(\Delta\phi_2, m_K L, a)$$
$$= \Delta_{B_{s0}^*/B_{s1}}(0, \infty, a)(1 + A\Delta\phi_2 + Be^{-m_K L}). \quad (17)$$

As in the $\ell s\bar{b}\bar{b}$ case, we share the fit parameters $\Delta_{B_{s0}^*/B_{s1}}(0, \infty, a)$ and B between our mass trajectories, and allow A to be a free parameter for each of them. We find the coefficient B to be very large, suggesting significant finite-volume effects are present in this quantity. The plots (15 and 16) of the effective masses (in Appendix D) show that even with our significant statistical resolution these quantities are noisy and often display large fluctuations in time.

The results for the two splittings at physical pion mass in the infinite-volume limit from our two different mass trajectories are (see Table XIII of Appendix C for more details):

$$\Delta_{B_{s0}^*}(0, \infty, a = 0.08636 \text{ fm}) = -68.5(3.0) \text{ [MeV]},$$
$$\Delta_{B_{s1}}(0, \infty, a = 0.08636 \text{ fm}) = -72.0(3.7) \text{ [MeV]}. \quad (18)$$

These fits have $\chi^2/\text{dof} = 0.8$ and 0.3, respectively. We considered fits with another free parameter multiplying higher-order powers of ϕ_2, but could not fit such expressions stably. We note that upon a cut of $m_K L > 5$ our results do not change within error.

We again convince ourselves that our largest systematics come from lattice-spacing artifacts. To further quantify our systematics we first consider the difference between the extrapolated results using the tree-level NRQCD prescription or various tunings to get the physical $B^* - B$ splitting right, but we find their effects to be negligible (discussed in Sec. VI). We then measure the

same quantities using the neural network tuning on ensemble H200 as an indication of the light-quark cutoff effects. We observe that half the difference between H200 and U103 is 6.85 Mev for the B_{s0}^* and 6.7 MeV for the B_{s1}, so we add that to the central values of Eq. (18) and quote the full difference as the systematic error. Unlike for the previous two tetraquark candidates, we will show in the next section in Fig. 11 that there is no dependence of these quantities on the $B^* - B$ splitting at the $SU(3)_f$-symmetric point, so we assume we do not have this associated systematic. For our final result we quote:

$$\Delta_{B_{s0}^*}(0, \infty, 0) = -75.4(3.0)_{\text{Stat}}(13.7)_a \text{ [MeV]},$$
$$\Delta_{B_{s1}}(0, \infty, 0) = -78.7(3.7)_{\text{Stat}}(13.4)_a \text{ [MeV]}. \quad (19)$$

These determinations equate to masses of $B_{s0}^* = 5698(14)$ and $B_{s1} = 5741(14)$ MeV for these states, where the isosymmetric kaon mass $m_K = 494.2$ MeV was used. Again, our leading systematic is our conservative estimate emanating from discretization effects.

VI. CROSS-CHECKS AND NRQCD SYSTEMATICS

At fixed bottomonium tuning, the measured $B^* - B$ splitting does not trend toward the physical result as the lattice spacing is decreased. As an alternative to our standard tuning, we are free in our philosophy to tune the NRQCD coefficients with the physical $B^* - B$ splitting as a parameter instead or in addition to the bottomonium hyperfine splitting. As a further possible choice, we also consider the tuning with the higher-order spin-dependent terms c_7, c_8, and c_9 of Eq. (3) set to their tree-level values. We will only perform this investigation on a single ensemble (U103) as this can be used to estimate a systematic for the $ud\bar{b}\bar{b}$ and $\ell s\bar{b}\bar{b}$ tetraquarks, or the B_{s0}^* and B_{s1} mesons.
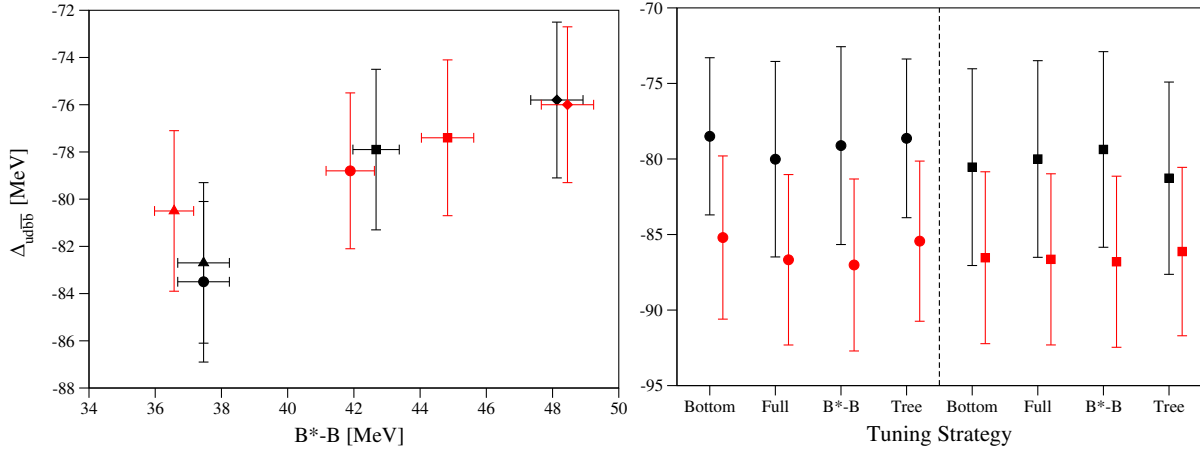
FIG. 11.   Left: $u d \bar{b} \bar{b}$ tetraquark binding-energy dependence on the $B^* - B$ hyperfine splitting using the extended tunings of Table XI. Red indicates that the tree-level spin-dependent $O(v^6)$ terms were used whereas black means $O(v^4)$, circles are our standard tuning, squares the "full" tuning, diamonds the $B^* - B$, and triangles the tree-level coefficients. Right: B_{s0}^* (black) and B_{s1} (red) binding-energy dependence on the tuning strategy; points on the right of the dashed line include spin-dependent $O(v^6)$ terms.

In Table XI we give the various nonperturbatively tuned coefficients we obtain with the inclusion of $O(v^4)$ and partial-$O(v^6)$ terms in the NRQCD Hamiltonian. The parameter c_7 has a somewhat strong impact on the kinetic mass and a complete retuning of the bare mass aM_0 was needed for the inclusion of the tree-level higher-order terms. Already we can see some patterns in the coefficients: for purely tuning the $B^* - B$ splitting the parameter c_4 is the most important and is in strong conflict with the pure-bottomonium tuning. The larger the value of c_4 the less negative the coefficient c_2 needs to become, suggesting there is a strong spin-independent contribution from c_4 that c_2 wants to counteract. At $O(v^4)$ c_1 and c_3 are positively correlated with c_4, an increase in c_4 increases both. Upon inclusion of tree-level $O(v^6)$ spin-dependent terms c_1 still grows with c_4 but now c_3 decreases.

The higher-order discretization-effect correction terms c_5 and c_6 are quite consistent within the range of predictions provided by the network. The variation on the Full tuning's parameters is always larger, suggesting that adding

an extra input that is in tension with the others produces worse results. Put another way: the network struggles to optimally determine the parameters that satisfy all the splittings used as inputs.

Figure 11 illustrates the dependence of the $u d \bar{b} \bar{b}$ tetraquark and the B_{s0}^* and B_{s1} meson binding energies on the $B^* - B$ hyperfine splitting. We note that there is a somewhat strong dependence on this splitting for the tetraquark and none for the exotic B mesons. For the tetraquarks in the previous section, we therefore shifted our final result and quantified the associated systematic uncertainty related to our $O(v^4)$ tuning. From Fig. 12 it is clear that we cannot simultaneously tune both the $\Upsilon - \eta_b$ and $B^* - B$ splittings to their physical value. There however seems to be convergence from tuning the pure-bottomonia spectrum with tree-level higher-order terms. With the addition of more states to tune against, or with the fixing of other terms to 1, it should be possible to also allow c_7 to vary to see whether these hyperfine splittings can be improved further.

TABLE XI.   Investigation of different tuning strategies and inclusion of higher-order spin-dependent terms of NRQCD for the ensemble U103. "Bottom" refers to our standard tuning while "$B^* - B$" refers to the tuning where the B-meson hyperfine splitting is used instead of the bottomonium hyperfine splitting, and "Full" refers to using both splittings.

| Tuning	aM_0	c_1	c_2	c_3	c_4	c_5	c_6	c_7	c_8	c_9
Bottom	1.8035(32)	0.787(16)	−0.789(61)	1.057(10)	0.960(11)	0.828(13)	0.932(14)	0	0	0
Full	1.8014(36)	0.791(25)	0.084(204)	1.061(10)	1.183(39)	0.860(19)	0.965(15)	0	0	0
$B^* - B$	1.8020(11)	0.838(7)	0.371(38)	1.073(5)	1.384(13)	0.831(9)	0.944(9)	0	0	0
Tree	1.8120(120)	1	1	1	1	1	1	0	0	0
Bottom	1.8643(20)	0.861(14)	−0.548(58)	1.134(18)	1.092(16)	0.810(19)	0.980(14)	1	1	1
Full	1.8612(24)	0.867(14)	−0.373(80)	1.100(16)	1.190(25)	0.821(12)	0.965(12)	1	1	1
$B^* - B$	1.8613(14)	0.895(10)	−0.167(40)	1.095(12)	1.312(9)	0.794(11)	0.946(9)	1	1	1
Tree	1.8825(110)	1	1	1	1	1	1	1	1	1
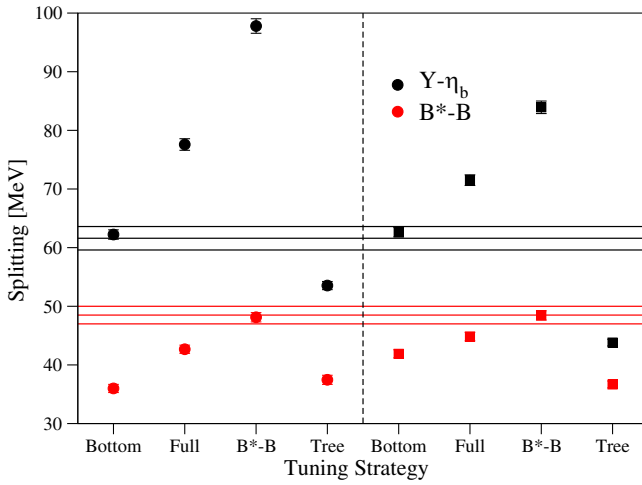
FIG. 12. Hyperfine splittings for the various tuning strategies and parameters in Table XI. The points left of the dashed line use the $O(v^4)$ NRQCD Hamiltonian, and those on the right include tree-level spin-dependent $O(v^6)$ terms. Horizontal lines give the PDG values for these splittings.

VII. CONCLUSIONS

We have shown it is possible to reproduce the experimental splittings of bottomonia with a simple lattice NRQCD prescription that has nonperturbatively tuned parameters from a neural network. We have investigated some of the S- and P-wave excited states of bottomonia in order to test our tuning and we find good consistency with experiment where available, and a more continuum-like behaviour of the bottomonium spectrum at finite lattice spacing. We have found that under our tuning the $B^* - B$ splitting is fairly far from the continuum result, with an indication that inclusion of higher-order spin-dependent terms improves the situation.

For all the heavy-light quantities we measured there was no discernible difference in the result from either using the tree-level NRQCD coefficients or those determined from a neural network using pure-bottomonium ground states. It could be possible that significant differences from the NRQCD prescription are largely canceled by the threshold subtractions performed for the states we investigated. The $B^* - B$ splitting does however have a significant impact on the doubly heavy tetraquark results.

Our physics objective was the calculation of the binding energy of the popular $I(J^P) = 0(1^+)$ $ud\bar{b}\bar{b}$, and $\frac{1}{2}(1^+)$ $\ell s\bar{b}\bar{b}$ tetraquark candidates. For the $ud\bar{b}\bar{b}$ tetraquark we find a strong-interaction-stable bound state 112.0(13.2) Mev below threshold, consistent with previous lattice studies. Our determination comes from a combined fit of ten different lattice ensembles with a large variation in pion mass and $m_\pi L$. We observe somewhat sizable finite-volume effects, $B^* - B$ mistuning effects, and most importantly discretization effects. The latter forms our largest systematic uncertainty. A future calculation of this state with a relativistic heavy-quark action to properly address this systematic is quite desirable.

The related $\ell s\bar{b}\bar{b}$ tetraquark candidate has typically been predicted by lattice studies to lie ≈ 90 MeV below the lowest-lying noninteracting two-meson threshold $(B_s B^*)$; here we measure this state to be only 46.4(12.3) MeV below it. As was the case for the $ud\bar{b}\bar{b}$, our result is dominated by our estimate of discretization systematics. Finite-volume effects are small and an $e^{-m_K L}$ term is slightly preferred for our range of $m_K L$. A comparison of our doubly heavy tetraquarks with other lattice determinations can be seen in Fig. 13; our measurements are at the bottom of the figures as they are all represented chronologically.

Finally, we investigated the B_{s0}^* and B_{s1} scalar and axial-vector B_s mesons in our setup and predict states 75.4(14.0) and 78.7(13.9) MeV below the corresponding BK and B^*K thresholds, respectively. Figure 14 shows a comparison to various lattice QCD and selected [142]
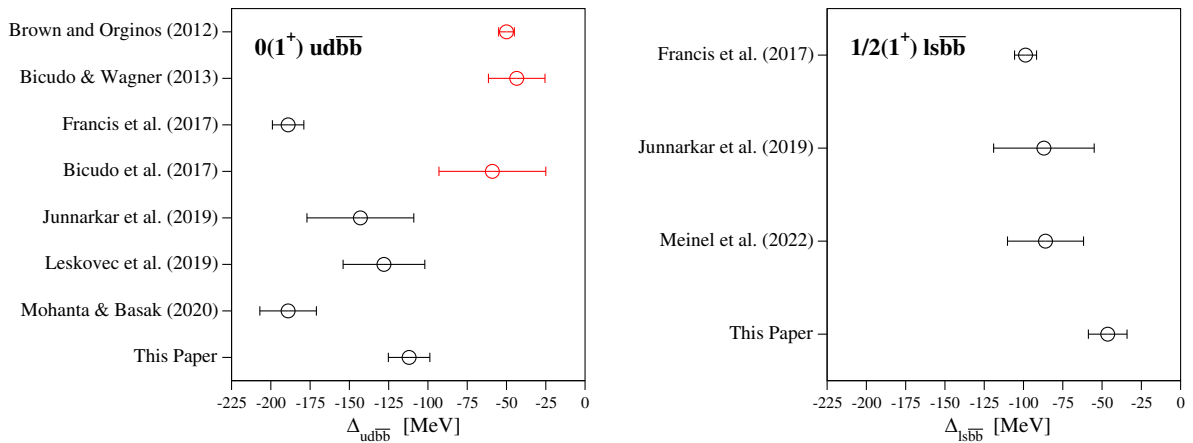

FIG. 13. Comparison plots of our result and other lattice QCD determinations for the $ud\bar{b}\bar{b}$ (left) and $\ell s\bar{b}\bar{b}$ (right) tetraquarks. Black circles indicate calculations performed with lattice NRQCD for the b quarks and red circles indicate the use of static b quarks. The years in parentheses are the publication dates of the papers. Statistical and systematic errors have been added in quadrature.
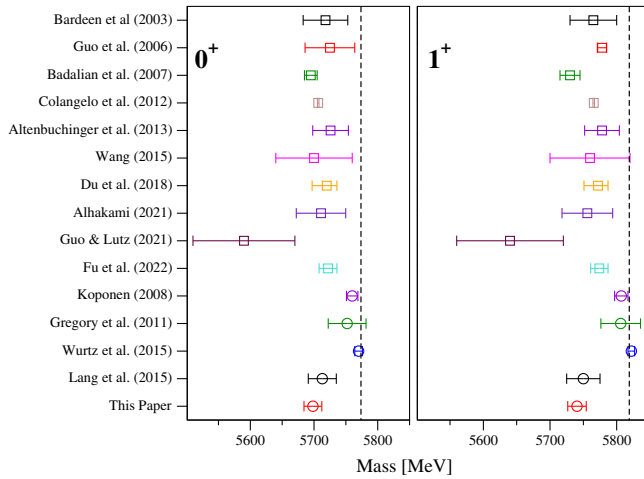
FIG. 14. Comparison of our results for the B_{s0}^* (left) and B_{s1} (right) ground-state masses to various other results. Circles denote the results of lattice calculations, while squares denote the results from model/Effective Field Theory (EFT) calculations. The vertical line denotes the respective threshold. To translate our result for the binding energy to the result displayed in this plot an isosymmetric kaon mass of 494.2 MeV has been used.

model/effective-field theory calculations. Our results are fully consistent with the previous pole determination of [53] and with most of the calculations based on effective field theory approaches and models based on chiral and heavy-quark symmetry. Our results however show tension with some of the previous heavy-light lattice NRQCD calculations, and we observe pretty significant finite-volume and pion-mass dependencies that must be taken into account in determining these states on the lattice. Our study has a very different approach from the previous works and different associated systematics. Hopefully further lattice QCD studies of these states will be performed in the future to clarify their masses in anticipation of an experimental determination.

The use of NRQCD is still relevant in the field of lattice QCD even as measurements with physical, dynamical b quarks are beginning to be performed. Lattice NRQCD is useful as a very cheap and statistically precise exploratory tool, but as it does not have a formal continuum limit one must ensure it is able to describe known states appropriately before performing physically relevant predictions. We argue this can be precisely done with our tuning at little extra expense, and comes with the minor loss of not having simple bottomonia states as predictions.

ACKNOWLEDGMENTS

APPENDIX A: TECHNICAL ASPECTS OF THE NRQCD CALCULATION

In this appendix we describe some of the details of our NRQCD implementation. Considering Eq. (2), it should be clear that the *natural* operations will be on $N_C \times N_C$ color matrices, so sink and source color indices will be the fastest moving in our propagator solution. Outer (spin) indices are considered as a matrix of size 2×2, i.e. the size of the Pauli matrices. We utilize the NRQCD implementation in [133], which is a pure thread-parallel (threaded using OpenMP [143] pragmas) application of the evolution equation [Eq. (1)] in a time slice by time slice manner. Aside from simple loop-unrolling and loop-fusion optimization strategies, this implementation applies all contributions (except H_0) of the Hamiltonian accumulated on the time slice into a buffer for better thread parallelism. As such, an important optimization is the precomputation of the combinations of links: $U_\mu(x + \frac{a}{2}\hat{\mu})U_\mu(x + 3\frac{a}{2}\hat{\mu})$, and of course the improved field-strength tensors. Such an optimization is necessary to avoid implicit thread barriers in OpenMP's parallel for routines, as they cost many CPU cycles. It turns out that these applications of the higher-order contributions from the Hamiltonian (δH) are the most costly parts of performing the evolution.

The majority of the NRQCD evolution algorithm can be boiled down to performing the product $A_{ab}S_{bc}^{\alpha\beta}$, i.e. a color matrix multiplied by a propagator (ab are inner color indices and $\alpha\beta$ the outer Dirac) and a specific, unrolled, advanced vector extensions/fused multiply-add (AVX/FMA) implementation is called that performs this operation reasonably optimally.

APPENDIX B: RETUNING WITH FIXED PARAMETERS

Here we detail an investigation into keeping the two higher-order lattice-spacing correction terms (c_5 and c_6) in the NRQCD action fixed to 1 and nonperturbatively tuning the others as one may be concerned with our setup having more outputs than inputs.

In Table XII we give the tuning parameters when $c_5 = c_6 = 1$. It seems that aM_0 is not greatly affected by this change; c_3 appears affected by a few %. We do see c_4 grow similarly, and c_1 tends closer to 1. c_2 remains strongly negative as all of the tuning runs have illustrated.

TABLE XII. Our nonperturbative tuning with c_5 and c_6 set to their tree-level values for the U_{0P} tadpole factor using ensemble A653. To be compared with our results in Table III.

aM_0	c_1	c_2	c_3	c_4	c_5	c_6
2.0583(6)	0.814(19)	−1.085(102)	1.145(11)	1.018(13)	1	1

c_1 and c_2 vary significantly compared to our full tuning. By not tuning c_5 and c_6 we obtain a worse percentage deviation [Eq. (6)] of 1.8% for our predicted values compared to the value of 0.7% in Table V. This mostly manifests in smaller splittings between the P-wave states. It is quite interesting that the range of neural network predictions for c_2 is so much larger than with the full seven-parameter tuning. This could be that the fit is trying to suppress higher-order spin-independent effects and tadpole factors directly with c_1 and c_2 as there is no longer freedom to do so with c_5 and c_6.

APPENDIX C: ON THE FINITE-VOLUME EFFECTS OF THE B_{s0}^* AND B_{s1} MESONS

Here we investigate further variations of the fits with regard to the finite-volume effects for the threshold-subtracted B_{s0}^* and B_{s1} mesons along the $\mathrm{Tr}[M] = C$ mass trajectory. Our preferred form is given by

$$\Delta_{B_{s0}^*/B_{s1}}(\phi_2, m_K L, a)$$
$$= \Delta_{B_{s0}^*/B_{s1}}(0, \infty, a)(1 + A\phi_2 + Ce^{-m_K L}), \quad \text{(C1)}$$

but it could be possible that this is subleading to a finite-volume term such as

$$\Delta_{B_{s0}^*/B_{s1}}(\phi_2, m_\pi L, a)$$
$$= \Delta_{B_{s0}^*/B_{s1}}(0, \infty, a)(1 + A\phi_2 + Ce^{-m_\pi L}), \quad \text{(C2)}$$

or even a combination of the two:

$$\Delta_{B_{s0}^*/B_{s1}}(\phi_2, m_K L, m_\pi L, a)$$
$$= \Delta_{B_{s0}^*/B_{s1}}(0, \infty, \infty, a)(1 + A\phi_2 + Be^{-m_K L} + Ce^{-m_\pi L}).$$
$$\text{(C3)}$$

TABLE XIII. Investigation of the combined chiral/finite-volume fits to the B_{s0}^* and B_{s1} mass differences along only the $\mathrm{Tr}[M] = C$ mass trajectory. "Combined" indicates that the results are from a simultaneous fit to both B_{s0}^* and B_{s1} mass differences, whereas "Individual" indicates fits individually to the data. "$m_K L$" indicates a fit to the form of Eq. (C1), "$m_\pi L$" to Eq. (C2), and "$m_\pi L + m_K L$" to Eq. (C3).

Fit	$\Delta_{B_{s0}^*}$ [MeV]	$\Delta_{B_{s1}}$ [MeV]	χ^2/dof
Combined $m_K L$	−67.5(3.4)	−71.9(3.8)	0.5
Combined $m_\pi L$	−54.7(4.1)	−58.4(4.6)	2.9
Combined $m_\pi L + m_K L$	−68.8(5.5)	−73.4(6.1)	0.5
Individual $m_K L$	−68.0(3.3)	−71.4(3.9)	0.9, 0.3
Individual $m_\pi L$	−55.3(3.9)	−57.6(4.8)	4.2, 2.8
Individual $m_\pi L + m_K L$	−70.1(5.4)	−72.0(6.2)	1.1, 0.3

We also note that in our individual fits the coefficients A and B are consistent with one another for both the B_{s0}^* and B_{s1}, so we consider a simultaneous fit with these (A, B, and C) parameters shared and the Δs free. We tabulate these results in Table XIII.

Table XIII illustrates that our data cannot be well described by a single $e^{-m_\pi L}$ finite-volume term, whereas any fit (combined or not) with an $m_K L$ term describes the data extremely well. We can include both $m_\pi L$ and $m_K L$ terms in our combined chiral/finite-volume fit but the result remains consistent with just the $m_K L$ form. In fact, the coefficient "C" is consistent with zero for these fits and typically the statistical error of the determination increases with no real improvement in fit quality. This suggests that $m_\pi L$ finite-volume effect terms serve only as nuisance parameters within the precision of our data, and we can safely conclude that they are subleading in both our B_{s0}^* and B_{s1} determinations.

APPENDIX D: EFFECTIVE MASSES—EXOTIC B_s MESONS

In this appendix we show the effective masses of our B_{s0}^* and B_{s1} data for all ensembles that enter the analysis.
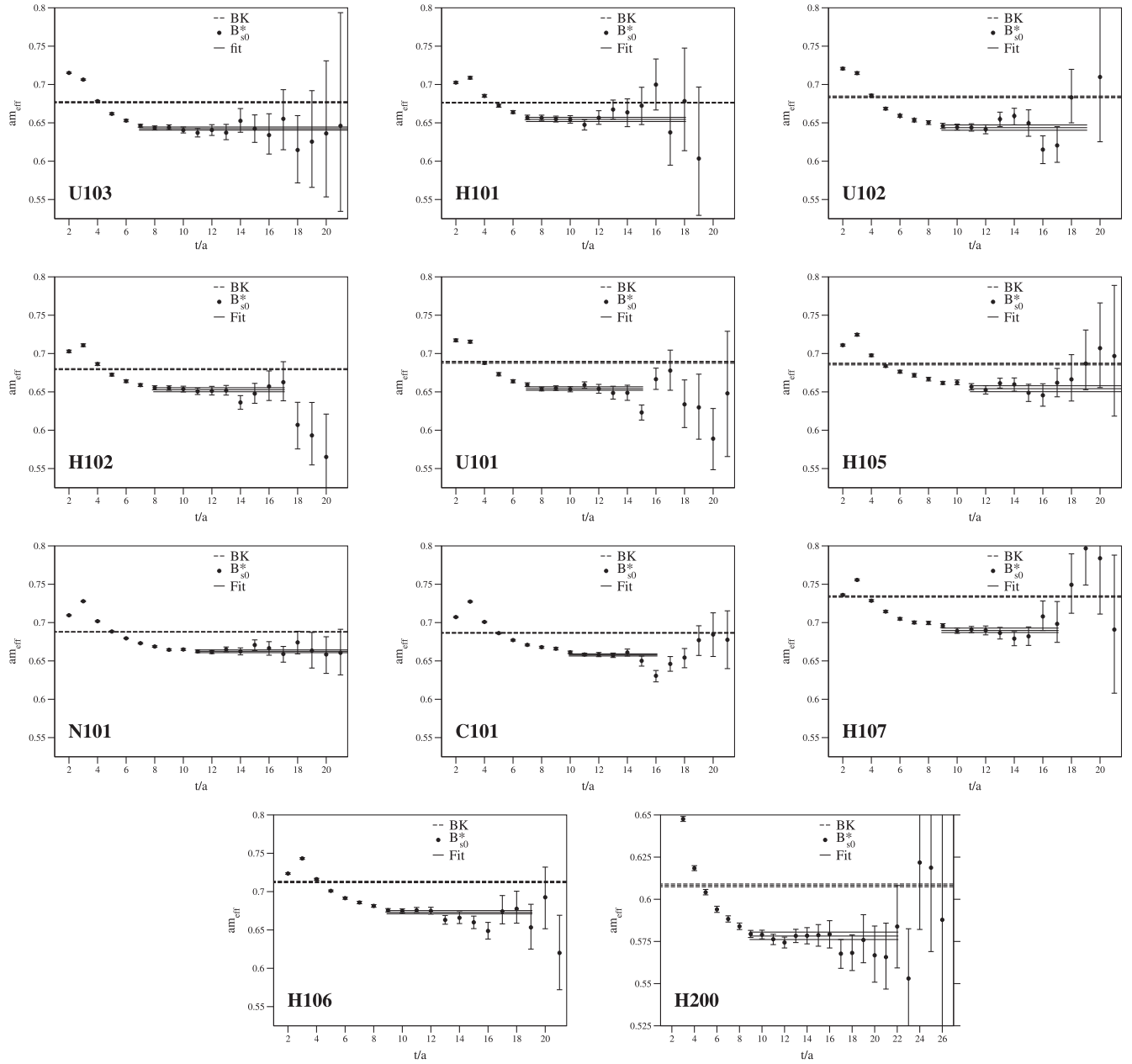
FIG. 15. Effective-mass plots of the B_{s0}^* meson with the measured (BK) threshold plotted. From left to right and top to bottom we show results from U103, H101, U102, H102, U101, H105, N101, C101, H107, H106, and H200.
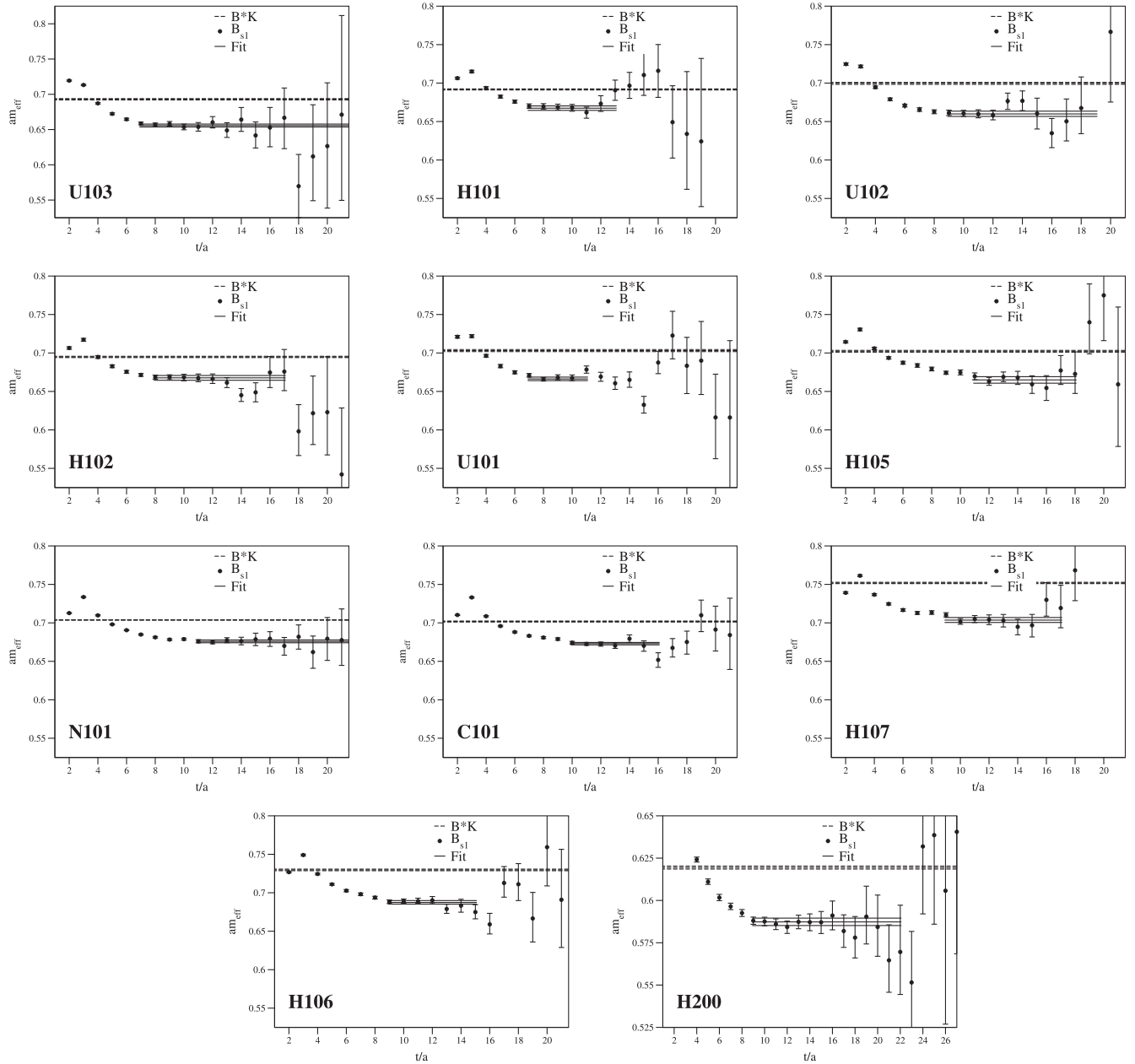
FIG. 16. Similarly to Fig. 15 but of the B_{s1} meson with the measured expected threshold (B^*K) plotted.

[1] P. Bicudo, K. Cichy, A. Peters, B. Wagenbach, and M. Wagner, Evidence for the existence of $ud\bar{b}\bar{b}$ and the nonexistence of $ss\bar{b}\bar{b}$ and $cc\bar{b}\bar{b}$ tetraquarks from lattice QCD, Phys. Rev. D **92**, 014507 (2015).

[2] A. Francis, R. J. Hudspith, R. Lewis, and K. Maltman, Lattice Prediction for Deeply Bound Doubly Heavy Tetraquarks, Phys. Rev. Lett. **118**, 142001 (2017).

[3] D. G. Richards, D. K. Sinclair, and D. W. Sivers, Lattice QCD simulation of meson exchange forces, Phys. Rev. D **42**, 3191 (1990).

[4] A. Mihaly, H. R. Fiebig, H. Markum, and K. Rabitsch, Interactions between heavy-light mesons in lattice QCD, Phys. Rev. D **55**, 3077 (1997).

[5] A. M. Green and P. Pennanen, An interquark potential model for multiquark systems, Phys. Rev. C **57**, 3384 (1998).

[6] C. Stewart and R. Koniuk, Hadronic molecules in lattice QCD, Phys. Rev. D **57**, 5581 (1998).

[7] P. Pennanen, C. Michael, and A. M. Green (UKQCD Collaboration), Interactions of heavy light mesons, Nucl. Phys. B Proc. Suppl. **83**, 200 (2000).

[8] W. Detmold, K. Orginos, and M. J. Savage, BB potentials in quenched lattice QCD, Phys. Rev. D **76,** 114503 (2007).

[9] Z. S. Brown and K. Orginos, Tetraquark bound states in the heavy-light heavy-light system, Phys. Rev. D **86,** 114506 (2012).

[10] M. Wagner (ETM Collaboration), Static-static-light-light tetraquarks in lattice QCD, Acta Phys. Pol. B Proc. Suppl. **4,** 747 (2011).

[11] P. Bicudo and M. Wagner (European Twisted Mass Collaboration), Lattice QCD signal for a bottom-bottom tetraquark, Phys. Rev. D **87,** 114511 (2013).

[12] P. Bicudo, K. Cichy, A. Peters, and M. Wagner, BB interactions with static bottom quarks from lattice QCD, Phys. Rev. D **93,** 034501 (2016).

[13] P. Bicudo, J. Scheunert, and M. Wagner, Including heavy spin effects in the prediction of a $\bar{b}\bar{b}ud$ tetraquark with lattice QCD potentials, Phys. Rev. D **95,** 034502 (2017).

[14] P. Junnarkar, N. Mathur, and M. Padmanath, Study of doubly heavy tetraquarks in lattice QCD, Phys. Rev. D **99,** 034507 (2019).

[15] L. Leskovec, S. Meinel, M. Pflaumer, and M. Wagner, Lattice QCD investigation of a doubly-bottom $\bar{b}\bar{b}ud$ tetraquark with quantum numbers $I(J^P) = 0(1^+)$, Phys. Rev. D **100,** 014503 (2019).

[16] P. Mohanta and S. Basak, Construction of $bb\bar{u}\bar{d}$ tetraquark states on lattice with NRQCD bottom and HISQ up and down quarks, Phys. Rev. D **102,** 094516 (2020).

[17] S. Zouzou, B. Silvestre-Brac, C. Gignoux, and J. M. Richard, Four quark bound states, Z. Phys. C **30,** 457 (1986).

[18] J. Carlson, L. Heller, and J. A. Tjon, Stability of dimesons, Phys. Rev. D **37,** 744 (1988).

[19] C. Semay and B. Silvestre-Brac, Diquonia and potential models, Z. Phys. C **61,** 271 (1994).

[20] S. Pepin, F. Stancu, M. Genovese, and J. M. Richard, Tetraquarks with color blind forces in chiral quark models, Phys. Lett. B **393,** 119 (1997).

[21] D. M. Brink and F. Stancu, Tetraquarks with heavy flavors, Phys. Rev. D **57,** 6778 (1998).

[22] J. Vijande, F. Fernandez, A. Valcarce, and B. Silvestre-Brac, Tetraquarks in a chiral constituent quark model, Eur. Phys. J. A **19,** 383 (2004).

[23] D. Ebert, R. N. Faustov, V. O. Galkin, and W. Lucha, Masses of tetraquarks with two heavy quarks in the relativistic quark model, Phys. Rev. D **76,** 114015 (2007).

[24] J. Vijande, E. Weissman, A. Valcarce, and N. Barnea, Are there compact heavy four-quark bound states?, Phys. Rev. D **76,** 094027 (2007).

[25] M. Zhang, H. X. Zhang, and Z. Y. Zhang, $QQ\bar{q}\bar{q}$ four-quark bound states in chiral SU(3) quark model, Commun. Theor. Phys. **50,** 437 (2008).

[26] S. H. Lee and S. Yasui, Stable multiquark states with heavy quarks in a diquark model, Eur. Phys. J. C **64,** 283 (2009).

[27] Y. Yang, C. Deng, J. Ping, and T. Goldman, S-wave $QQ\bar{q}\bar{q}$ state in the constituent quark model, Phys. Rev. D **80,** 114023 (2009).

[28] Z.-G. Wang, Analysis of the axialvector doubly heavy tetraquark states with QCD sum rules, Acta Phys. Pol. B **49,** 1781 (2018).

[29] M. Karliner and J. L. Rosner, Discovery of Doubly-Charmed Ξ_{cc} Baryon Implies a Stable ($bb\bar{u}\bar{d}$) Tetraquark, Phys. Rev. Lett. **119,** 202001 (2017).

[30] E. J. Eichten and C. Quigg, Heavy-Quark Symmetry Implies Stable Heavy Tetraquark Mesons $Q_iQ_j\bar{q}_k\bar{q}_l$, Phys. Rev. Lett. **119,** 202002 (2017).

[31] A. Czarnecki, B. Leng, and M. B. Voloshin, Stability of tetrons, Phys. Lett. B **778,** 233 (2018).

[32] T. Mehen, Implications of heavy quark-diquark symmetry for excited doubly heavy baryons and tetraquarks, Phys. Rev. D **96,** 094028 (2017).

[33] L. Maiani, A. D. Polosa, and V. Riquer, Hydrogen bond of QCD in doubly heavy baryons and tetraquarks, Phys. Rev. D **100,** 074002 (2019).

[34] E. Hernández, J. Vijande, A. Valcarce, and J.-M. Richard, Spectroscopy, lifetime and decay modes of the T_{bb}^- tetraquark, Phys. Lett. B **800,** 135073 (2020).

[35] Q.-F. Lü, D.-Y. Chen, and Y.-B. Dong, Masses of doubly heavy tetraquarks $T_{QQ'}$ in a relativized quark model, Phys. Rev. D **102,** 034012 (2020).

[36] E. Braaten, L.-P. He, and A. Mohapatra, Masses of doubly heavy tetraquarks with error bars, Phys. Rev. D **103,** 016001 (2021).

[37] J.-B. Cheng, S.-Y. Li, Y.-R. Liu, Z.-G. Si, and T. Yao, Double-heavy tetraquark states with heavy diquark-antiquark symmetry, Chin. Phys. C **45,** 043102 (2021).

[38] Q. Meng, E. Hiyama, A. Hosaka, M. Oka, P. Gubler, K. U. Can, T. T. Takahashi, and H. S. Zong, Stable double-heavy tetraquarks: Spectrum and structure, Phys. Lett. B **814,** 136095 (2021).

[39] X.-Z. Weng, W.-Z. Deng, and S.-L. Zhu, Doubly heavy tetraquarks in an extended chromomagnetic model, Chin. Phys. C **46,** 013102 (2022).

[40] R. N. Faustov, V. O. Galkin, and E. M. Savchenko, Heavy tetraquarks in the relativistic quark model, Universe **7,** 94 (2021).

[41] C. Deng and S.-L. Zhu, Tcc+ and its partners, Phys. Rev. D **105,** 054015 (2022).

[42] T. Guo, J. Li, J. Zhao, and L. He, Mass spectra of doubly heavy tetraquarks in an improved chromomagnetic inter-action model, Phys. Rev. D **105,** 014021 (2022).

[43] Y. Kim, M. Oka, and K. Suzuki, Doubly heavy tetraquarks in a chiral-diquark picture, Phys. Rev. D **105,** 074021 (2022).

[44] S. Meinel, M. Pflaumer, and M. Wagner, Search for $\bar{b}\bar{b}us$ and $\bar{b}\bar{c}ud$ tetraquark bound states using lattice QCD, Phys. Rev. D **106,** 034507 (2022).

[45] B. Silvestre-Brac and C. Semay, Systematics of $L = 0q^2\bar{q}^2$ systems, Z. Phys. C **57,** 273 (1993).

[46] M.-L. Du, W. Chen, X.-L. Chen, and S.-L. Zhu, Exotic $QQ\bar{q}\bar{q}$, $QQ\bar{q}\bar{s}$ and $QQ\bar{s}\bar{s}$ states, Phys. Rev. D **87,** 014003 (2013).

[47] W. Park, S. Noh, and S. H. Lee, Masses of the doubly heavy tetraquarks in a constituent quark model, Nucl. Phys. **A983,** 1 (2019).

[48] C. Deng, H. Chen, and J. Ping, Systematical investigation on the stability of doubly heavy tetraquark states, Eur. Phys. J. A **56,** 9 (2020).

[49] L. R. Dai, E. Oset, A. Feijoo, R. Molina, L. Roca, A. M. Torres, and K. P. Khemchandani, Masses and widths of the

exotic molecular B(s)(*)B(s)(*) states, Phys. Rev. D **105**, 074017 (2022); **106**, 099904(E) (2022).

[50] S. Godfrey and N. Isgur, Mesons in a relativized quark model with chromodynamics, Phys. Rev. D **32**, 189 (1985).

[51] B. Aubert *et al.* (*BABAR* Collaboration), Observation of a Narrow Meson Decaying to $D_s^+ \pi^0$ at a Mass of 2.32 GeV/c^2, Phys. Rev. Lett. **90**, 242001 (2003).

[52] D. Besson *et al.* (CLEO Collaboration), Observation of a narrow resonance of mass 2.46 GeV/c^2 decaying to $D_s^{*+} \pi^0$ pi0 and confirmation of the D*(sJ)(2317) state, Phys. Rev. D **68**, 032002 (2003); **75**, 119908(E) (2007).

[53] C. B. Lang, D. Mohler, S. Prelovsek, and R. M. Woloshyn, Predicting positive parity B_s mesons from lattice QCD, Phys. Lett. B **750**, 17 (2015).

[54] E. B. Gregory *et al.*, Precise B, B_s and B_c meson spectroscopy from full lattice QCD, Phys. Rev. D **83**, 014506 (2011).

[55] M. Wurtz, R. Lewis, and R. M. Woloshyn, Free-form smearing for bottomonium and B meson spectroscopy, Phys. Rev. D **92**, 054504 (2015).

[56] J. Koponen (UKQCD), Energies of B_s meson excited states: A lattice study, Phys. Rev. D **78**, 074509 (2008).

[57] A. H. Orsland and H. Hogaasen, Strong and electromagnetic decays for excited heavy mesons, Eur. Phys. J. C **9**, 503 (1999).

[58] W. A. Bardeen, E. J. Eichten, and C. T. Hill, Chiral multiplets of heavy-light mesons, Phys. Rev. D **68**, 054024 (2003).

[59] E. E. Kolomeitsev and M. F. M. Lutz, On heavy light meson resonances and chiral symmetry, Phys. Lett. B **582**, 39 (2004).

[60] T. Matsuki, K. Mawatari, T. Morii, and K. Sudoh, 0^+ and 1^+ states of B and B_s mesons, Phys. Lett. B **606**, 329 (2005).

[61] F.-K. Guo, P.-N. Shen, H.-C. Chiang, R.-G. Ping, and B.-S. Zou, Dynamically generated 0+ heavy mesons in a heavy chiral unitary approach, Phys. Lett. B **641**, 278 (2006).

[62] F.-K. Guo, P.-N. Shen, and H.-C. Chiang, Dynamically generated 1+ heavy mesons, Phys. Lett. B **647**, 133 (2007).

[63] A. M. Badalian, Y. A. Simonov, and M. A. Trusov, The chiral transitions in heavy-light mesons, Phys. Rev. D **77**, 074017 (2008).

[64] J. Vijande, A. Valcarce, and F. Fernandez, B meson spectroscopy, Phys. Rev. D **77**, 017501 (2008).

[65] M. Cleven, F.-K. Guo, C. Hanhart, and U.-G. Meissner, Light meson mass dependence of the positive parity heavy-strange mesons, Eur. Phys. J. A **47**, 19 (2011).

[66] V. Dmitrasinovic, Chiral symmetry of heavy-light scalar mesons with $U_A(1)$ symmetry breaking, Phys. Rev. D **86**, 016006 (2012).

[67] P. Colangelo, F. De Fazio, F. Giannuzzi, and S. Nicotri, New meson spectroscopy with open charm and beauty, Phys. Rev. D **86**, 054024 (2012).

[68] M. Altenbuchinger, L. S. Geng, and W. Weise, Scattering lengths of Nambu-Goldstone bosons off D mesons and dynamically generated heavy-light mesons, Phys. Rev. D **89**, 014026 (2014).

[69] J. M. Torres-Rincon, L. Tolos, and O. Romanets, Open bottom states and the $\bar{B}$-meson propagation in hadronic matter, Phys. Rev. D **89**, 074042 (2014).

[70] Z.-G. Wang, Analysis of the masses and decay constants of the heavy-light mesons with QCD sum rules, Eur. Phys. J. C **75**, 427 (2015).

[71] P. G. Ortega, J. Segovia, D. R. Entem, and F. Fernández, Threshold effects in P-wave bottom-strange mesons, Phys. Rev. D **95**, 034010 (2017).

[72] M. Albaladejo, P. Fernandez-Soler, J. Nieves, and P. G. Ortega, Lowest-lying even-parity $\bar{B}_s$ mesons: Heavy-quark spin-flavor symmetry, chiral dynamics, and constituent quark-model bare masses, Eur. Phys. J. C **77**, 170 (2017).

[73] H.-Y. Cheng and F.-S. Yu, Masses of scalar and axial-vector B mesons revisited, Eur. Phys. J. C **77**, 668 (2017).

[74] M.-L. Du, M. Albaladejo, P. Fernández-Soler, F.-K. Guo, C. Hanhart, U.-G. Meißner, J. Nieves, and D.-L. Yao, Towards a new paradigm for heavy-light meson spectroscopy, Phys. Rev. D **98**, 094018 (2018).

[75] M. H. Alhakami, Predictions for the beauty meson spectrum, Phys. Rev. D **103**, 034009 (2021).

[76] H.-L. Fu, H. W. Grießhammer, F.-K. Guo, C. Hanhart, and U.-G. Meißner, Update on strong and radiative decays of the $D_{s0}^*(2317)$ and $D_{s1}(2460)$ and their bottom cousins, Eur. Phys. J. A **58**, 70 (2022).

[77] Z. Yang, G.-J. Wang, J.-J. Wu, M. Oka, and S.-L. Zhu, The investigations of the P-wave B_s states combining quark model and lattice QCD in the coupled channel framework, J. High Energy Phys. 01 (2023) 058.

[78] S. Godfrey and R. Kokoski, The properties of p wave mesons with one heavy quark, Phys. Rev. D **43**, 1679 (1991).

[79] T. A. Lahde, C. J. Nyfalt, and D. O. Riska, Spectra and M1 decay widths of heavy light mesons, Nucl. Phys. **A674**, 141 (2000).

[80] M. Di Pierro and E. Eichten, Excited heavy-light systems and hadronic transitions, Phys. Rev. D **64**, 114004 (2001).

[81] O. Lakhina and E. S. Swanson, A canonical Ds(2317)?, Phys. Lett. B **650**, 159 (2007).

[82] D. Ebert, R. N. Faustov, and V. O. Galkin, Heavy-light meson spectroscopy and Regge trajectories in the relativistic quark model, Eur. Phys. J. C **66**, 197 (2010).

[83] Y. Sun, Q.-T. Song, D.-Y. Chen, X. Liu, and S.-L. Zhu, Higher bottom and bottom-strange mesons, Phys. Rev. D **89**, 054026 (2014).

[84] S. Godfrey, K. Moats, and E. S. Swanson, B and B_s meson spectroscopy, Phys. Rev. D **94**, 054025 (2016).

[85] C. McNeile, C. T. H. Davies, E. Follana, K. Hornbostel, and G. P. Lepage, High-precision c and b masses, and QCD coupling from current-current correlators in lattice and continuum QCD, Phys. Rev. D **82**, 034512 (2010).

[86] C. T. H. Davies, K. Hornbostel, A. Langnau, G. P. Lepage, A. Lidsey, C. J. Morningstar, J. Shigemitsu, and J. H. Sloan, New Determination of M(b) Using Lattice QCD, Phys. Rev. Lett. **73**, 2654 (1994).

[87] A. Gray, I. Allison, C. T. H. Davies, E. Dalgic, G. P. Lepage, J. Shigemitsu, and M. Wingate, Υ spectrum and m_b from full lattice QCD, Phys. Rev. D **72**, 094507 (2005).

[88] H. Na, C. M. Bouchard, G. P. Lepage, C. Monahan, and J. Shigemitsu (HPQCD), $B \to Dl\nu$ form factors at nonzero recoil and extraction of $|V_{cb}|$, Phys. Rev. D **92,** 054510 (2015); **93,** 119906(E) (2016).

[89] A. X. El-Khadra, A. S. Kronfeld, and P. B. Mackenzie, Massive fermions in lattice gauge theory, Phys. Rev. D **55,** 3933 (1997).

[90] N. H. Christ, M. Li, and H.-W. Lin, Relativistic heavy quark effective action, Phys. Rev. D **76,** 074505 (2007).

[91] M. B. Oktay and A. S. Kronfeld, New lattice action for heavy quarks, Phys. Rev. D **78,** 014504 (2008).

[92] J. Heitger and R. Sommer (ALPHA Collaboration), Non-perturbative heavy quark effective theory, J. High Energy Phys. 02 (2004) 022.

[93] B. Blossier et al. (ETM Collaboration), A proposal for B-physics on current lattices, J. High Energy Phys. 04 (2010) 049.

[94] W. G. Parrott, C. Bouchard, C. T. H. Davies, and D. Hatton, Toward accurate form factors for B-to-light meson decay from lattice QCD, Phys. Rev. D **103,** 094506 (2021).

[95] B. Colquhoun, S. Hashimoto, T. Kaneko, and J. Koponen (JLQCD Collaboration), Form factors of $B \to \pi\ell\nu$ and a determination of $|V_{ub}|$ with Möbius domain-wall fermions, Phys. Rev. D **106,** 054502 (2022).

[96] G. P. Lepage, L. Magnea, C. Nakhleh, U. Magnea, and K. Hornbostel, Improved nonrelativistic QCD for heavy quark physics, Phys. Rev. D **46,** 4052 (1992).

[97] S. Meinel, Bottomonium spectrum at order v^6 from domain-wall lattice QCD: Precise results for hyperfine splittings, Phys. Rev. D **82,** 114502 (2010).

[98] C. T. H. Davies, J. Harrison, C. Hughes, R. R. Horgan, G. M. von Hippel, and M. Wingate, Improving the kinetic couplings in lattice nonrelativistic QCD, Phys. Rev. D **99,** 054502 (2019).

[99] G. P. Lepage and P. B. Mackenzie, On the viability of lattice perturbation theory, Phys. Rev. D **48,** 2250 (1993).

[100] P. Lepage, Perturbative improvement for lattice QCD: An update, Nucl. Phys. B Proc. Suppl. **60,** 267 (1998).

[101] C. J. Morningstar, Radiative corrections to the kinetic couplings in nonrelativistic lattice QCD, Phys. Rev. D **50,** 5902 (1994).

[102] C. J. Morningstar, The heavy quark self-energy in non-relativistic lattice QCD, Phys. Rev. D **48,** 2265 (1993).

[103] N. Mathur, R. Lewis, and R. M. Woloshyn, Charmed and bottom baryons from lattice NRQCD, Phys. Rev. D **66,** 014502 (2002).

[104] As we will use a mix of periodic and open boundary condition ensembles in time, we will look at a single, coarse, periodic box to do this comparison.

[105] R. J. Dowdall, C. T. H. Davies, T. C. Hammant, and R. R. Horgan, Precise heavy-light meson masses and hyperfine splittings from lattice QCD including charm quarks in the sea, Phys. Rev. D **86,** 094510 (2012).

[106] A. V. Manohar, The HQET/NRQCD Lagrangian to order α_s/m^3, Phys. Rev. D **56,** 230 (1997).

[107] R. Lewis and R. M. Woloshyn, $O(1/M^3)$ effects for heavy-light mesons in lattice NRQCD, Phys. Rev. D **58,** 074506 (1998).

[108] C. Hughes, R. J. Dowdall, C. T. H. Davies, R. R. Horgan, G. von Hippel, and M. Wingate, Hindered M1 radiative decay of $\Upsilon(2S)$ from lattice NRQCD, Phys. Rev. D **92,** 094501 (2015).

[109] S. Meinel, Excited-state spectroscopy of triply-bottom baryons from lattice QCD, Phys. Rev. D **85,** 114510 (2012).

[110] T. C. Hammant, A. G. Hart, G. M. von Hippel, R. R. Horgan, and C. J. Monahan, Radiative Improvement of the Lattice NRQCD Action Using the Background Field Method and Application to the Hyperfine Splitting of Quarkonium States, Phys. Rev. Lett. **107,** 112002 (2011); **115,** 039901(E) (2015).

[111] T. C. Hammant, A. G. Hart, G. M. von Hippel, R. R. Horgan, and C. J. Monahan, Radiative improvement of the lattice nonrelativistic QCD action using the background field method with applications to quarkonium spectroscopy, Phys. Rev. D **88,** 014505 (2013); **92,** 119904(E) (2015).

[112] P. F. Bedaque, Aharonov-Bohm effect and nucleon nucleon phase shifts on the lattice, Phys. Lett. B **593,** 82 (2004).

[113] C. T. Sachrajda and G. Villadoro, Twisted boundary conditions in lattice simulations, Phys. Lett. B **609,** 73 (2005).

[114] C. T. H. Davies, K. Hornbostel, A. Langnau, G. P. Lepage, A. Lidsey, J. Shigemitsu, and J. H. Sloan, Precision Υ spectroscopy from nonrelativistic lattice QCD, Phys. Rev. D **50,** 6963 (1994).

[115] Fixed to a precision of 10^{-14} using the FACG algorithm [144].

[116] P. Zyla et al. (Particle Data Group), Review of particle physics, Prog. Theor. Exp. Phys. **2020,** 083C01 (2020).

[117] C. T. H. Davies et al. (HPQCD, UKQCD, MILC, Fermilab Lattice Collaborations), High Precision Lattice QCD Confronts Experiment, Phys. Rev. Lett. **92,** 022001 (2004).

[118] S. Meinel, Bottomonium spectrum from lattice QCD with $2+1$ flavors of domain wall fermions, Phys. Rev. D **79,** 094501 (2009).

[119] R. J. Hudspith and D. Mohler, A fully non-perturbative charm-quark tuning using machine learning, Phys. Rev. D **106,** 034508 (2022).

[120] D. P. Kingma and J. Ba, Adam: A method for stochastic optimization (2014), cite arxiv:1412.6980, Published as a conference paper at the 3rd International Conference for Learning Representations, San Diego, 2015.

[121] This was tested on our lightest pion-mass ensemble (C101) to be the case.

[122] M. Luscher and S. Schaefer, Lattice QCD with open boundary conditions and twisted-mass reweighting, Comput. Phys. Commun. **184,** 519 (2013).

[123] M. Bruno et al., Simulation of QCD with $N_f = 2 + 1$ flavors of non-perturbatively improved Wilson fermions, J. High Energy Phys. 02 (2015) 043.

[124] M. Bruno, T. Korzec, and S. Schaefer, Setting the scale for the CLS $2 + 1$ flavor ensembles, Phys. Rev. D **95,** 074504 (2017).

[125] E.-H. Chao, R. J. Hudspith, A. Gérardin, J. R. Green, H. B. Meyer, and K. Ottnad, Hadronic light-by-light contribution to $(g-2)_\mu$ from lattice QCD: A complete calculation, Eur. Phys. J. C **81,** 651 (2021).

[126] C. Michael and I. Teasdale, Extracting glueball masses from lattice QCD, Nucl. Phys. **B215,** 433 (1983).

[127] M. Luscher and U. Wolff, How to calculate the elastic scattering matrix in two-dimensional quantum field theories by numerical simulation, Nucl. Phys. **B339,** 222 (1990).

[128] B. Blossier, M. Della Morte, G. von Hippel, T. Mendes, and R. Sommer, On the generalized eigenvalue method for energies and matrix elements in lattice field theory, J. High Energy Phys. 04 (2009) 094.

[129] C. McNeile and C. Michael (UKQCD Collaboration), The η and η' mesons in QCD, Phys. Lett. B **491,** 123 (2000); **551,** 391(E) (2003).

[130] W. Bietenholz *et al.*, Tuning the strange quark mass in lattice simulations, Phys. Lett. B **690,** 436 (2010).

[131] G. S. Bali, E. E. Scholz, J. Simeth, and W. Söldner (RQCD Collaboration), Lattice simulations with $N_f = 2 + 1$ improved Wilson fermions at a fixed strange quark mass, Phys. Rev. D **94,** 074501 (2016).

[132] G. S. Bali, S. Collins, P. Georg, D. Jenkins, P. Korcyl, A. Schäfer, E. E. Scholz, J. Simeth, W. Söldner, and S. Weishäupl (RQCD Collaboration), Scale setting and the light baryon spectrum in $N_f = 2 + 1$ QCD with Wilson fermions, J. High Energy Phys. 05 (2023) 035.

[133] R. J. Hudspith, B. Colquhoun, A. Francis, R. Lewis, and K. Maltman, A lattice investigation of exotic tetraquark channels, Phys. Rev. D **102,** 114506 (2020).

[134] A. Francis, J. R. Green, P. M. Junnarkar, C. Miao, T. D. Rae, and H. Wittig, Lattice QCD study of the H dibaryon using hexaquark and two-baryon interpolators, Phys. Rev. D **99,** 074505 (2019).

[135] C. Aubin and K. Orginos, A new approach for Delta form factors, AIP Conf. Proc. **1374,** 621 (2011).

[136] J. R. Green, J. W. Negele, A. V. Pochinsky, S. N. Syritsyn, M. Engelhardt, and S. Krieg, Nucleon electromagnetic form factors from lattice QCD using a nearly physical pion mass, Phys. Rev. D **90,** 074507 (2014).

[137] S. Aoki *et al.*, Review of lattice results concerning low-energy particle physics, Eur. Phys. J. C **77,** 112 (2017).

[138] Y. Aoki *et al.* (Flavour Lattice Averaging Group (FLAG)), FLAG review 2021, Eur. Phys. J. C **82,** 869 (2022).

[139] We tested that using the CLS continuum value of t_0 instead produces a negligible shift in our final result.

[140] Neglecting the tiny differences in volume and pion mass between these two ensembles.

[141] On this particular ensemble BK and B^*K are the same as $B\pi$ and $B^*\pi$.

[142] We chose the references that attempt to quantify the uncertainty of the calculation. References [72] and [77] use lattice QCD input and are not fully independent of previous lattice results and so we therefore mention them here instead of in the overview plot. The results from [65] are superseded by the results in [76] and we therefore omit the former from the overview plot.

[143] L. Dagum and R. Menon, Openmp: An industry standard API for shared-memory programming, IEEE Comput. Sci. Eng. **5,** 46 (1998).

[144] R. J. Hudspith (RBC, UKQCD Collaborations), Fourier accelerated conjugate gradient lattice gauge fixing, Comput. Phys. Commun. **187,** 115 (2015).